Unclassified
Security Classification

AD-749547

DOCUMENT CONTROL DATA - R & D

(Security classification of title, body of abstract and indexing annotation must be entered when the overall report is classified)

1. ORIGINATING ACTIVITY (Corporate author)
University of Cincinnati

2a. REPORT SECURITY CLASSIFICATION
Unclassified

2b. GROUP
NA

3. REPORT TITLE
Calculation of Particle Trajectories in a Stationary Two Dimensional Cascade

4. DESCRIPTIVE NOTES (Type of report and inclusive dates)
Technical Report

5. AUTHOR(S) (First name, middle initial, last name)
M.F. Hussein and W. Tabakoff

6. REPORT DATE
June 1972

7a. TOTAL NO. OF PAGES
50

7b. NO. OF REFS
18

8a. CONTRACT OR GRANT NO.
DAHC04-69-C-0016

b. PROJECT NO.

c.

d.

9a. ORIGINATOR'S REPORT NUMBER(S)
Project Themis Report No. 72-27

9b. OTHER REPORT NO(S) (Any other numbers that may be assigned this report)
ARO D-T-4.44-E

10. DISTRIBUTION STATEMENT
Distribution of this report is unlimited

11. SUPPLEMENTARY NOTES
None

12. SPONSORING MILITARY ACTIVITY
U.S. Army Research Office - Durham
Box CM, Duke Station
Durham, North Carolina 27706

13. ABSTRACT

The trajectories of solid particles entrained by fluid flow in turbine and compressor stators were calculated. The impact and rebound phenomena of the solid particles was investigated experimentally and then considered in the solution of the equations of motion of the solid particles. The effect of the particle mean diameter, material density, and initial particle and gas velocities on the dynamic behavior of the solid particles through the cascade channel was also investigated. In addition, this study yielded information concerning blade erosion damage.

Key Words

Turbomachinery

Solid Particle Trajectories

DD FORM 1473 (PAGE 1) REPLACES DD FORM 1473, 1 JAN 68, WHICH IS OBSOLETE FOR ARMY USE.

Unclassified
Security Classification

PROJECT THEMIS REPORT NO. 72-27

CALCULATION OF PARTICLE TRAJECTORIES IN A STATIONARY TWO DIMENSIONAL CASCADE

M.F. Hussein and W. Tabakoff

June 1972

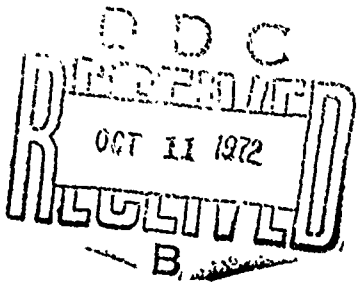

This work was supported by the U.S. Army Research Office - Durham under Project Themis Contract Number DAHC04-69-C-0016.

DEPARTMENT OF AEROSPACE ENGINEERING

University of Cincinnati, Cincinnati, Ohio 45221

12

TABLE OF CONTENTS

LIST OF ILLUSTRATIONS

NOMENCLATURE

Symbols

$\bar{a}$	particle acceleration
α	particle concentration
$\bar{\alpha}$	particle angular acceleration
B	reference frame fixed in blades
$\bar{b}$	position vector of a particle in B
β	angle between particle velocity and tangent to blade surface
β_i, β_{out}	gas flow inlet and outlet direction measured from the x axis
C	coefficient inversely proportional to particle characteristic time
$\bar{c}$	position vector of the origin of x,y,z axes relative to the axes fixed in E
C_D	drag coefficient
C_{D_o}	drag coefficient at Reynolds number less than 1.0
C_p	specific heat of gas at constant pressure
$\bar{D}$	drag force on the particles
d_p	particle mean diameter
Δt	increment of time
E	reference frame fixed in space
E_o	origin of the axes X,Y,Z fixed in E
$\bar{e}$	position vector of p relative to axes fixed in E
F	components of the drag force on the particles
g(Re)	correction function for the drag on sphere
h	blade height

Symbols

m_p	mass of one particle
μ_g	gas viscosity
$\bar{n}_1, \bar{n}_2, \bar{n}_3$	unit vectors in the direction of x,y,z axes
$\bar{N}_1, \bar{N}_2, \bar{N}_3$	unit vectors in the direction of X,Y,Z axes
p	pressure force on spherical particles
R	mean radius from axis of symmetry of cascade
Re	Reynolds number
s	angular blade spacing
t	time
T_{g_o}	total gas temperature
u	velocity in x direction
v	velocity in y direction
V	velocity relative to blade
w	velocity in z direction
x,y,z	axes fixed in B
X,Y,Z	axes fixed in E
ω	blade angular velocity
ψ	a form of the stream function

Subscripts

1	before collision
2	after collision
g	gas
i	inlet to stator
n	normal to surface
out	outlet from stator

Subscripts (continued)

p	particles
t	tangent to surface
x	in the x direction
y	in the y direction
z	in the z direction

Superscripts

B	relative to B
B_o	the origin of the axes x,y,z fixed in B
E	relative to E
p	particle position
p*	a point that coincides with p at a certain instance of time

ABSTRACT

The trajectories of solid particles entrained by fluid flow in turbine and compressor stators were calculated. The impact and rebound phenomena of the solid particles was investigated experimentally and then considered in the solution of the equations of motion of the solid particles. The effect of the particle mean diameter, material density, and initial particle and gas velocities on the dynamic behavior of the solid particles through the cascade channel was also investigated. In addition, this study yielded information concerning blade erosion damage.

INTRODUCTION

This investigation was undertaken to determine a theoretical approach to calculate the dynamic behavior of solid particles entrained by a gas flow in a two-dimensional stationary cascade of a turbine or a compressor blading. By dynamic behavior, it is meant the x-y location of the particles at any time in the cascade channel, that is, the path they follow and their velocity history through the passage taking into consideration both their collision with the blade surface and subsequent rebound from it.

The equations of motion of solid particles moving in a stream of gas were formulated assuming that the only force exerted is the drag force which causes the particles acceleration. In order to determine the solution to the equations of motion, information about the gas properties in the channel, the drag coefficient for spherical particles, the restitution ratio, and the rebound to incidence angle ratio were required.

The properties of the gas were calculated at all points of a square grid by solving numerically the equations of motion of gas flow in a cascade. The gas properties were assumed to be unchanged due to the presence of solid particles.

Drag coefficient formulas for spherical particles were determined for different ranges of Reynolds number based on particle mean diameter and the velocity difference between the gas and particle. Extensive experimental data were collected to study the collision and rebound phenomena of the particles with the blade's wall.

Formulas to determine the restitution ratio, that is, the ratio between particle velocities after and before collision, and the rebound to collision angle ratio were required. This is necessary because the points of collision are points of discontinuity, and hence, new initial conditions are required to continue the solution of the equations of motion. These experimentally correlated formulas are dependent on both the blade material and the particle material and shape, and may have different forms for different combinations of these. However, the order of magnitude of these ratios are the same, a fact that ensures the reliability of the results of this investigation. Once the operating conditions of an engine are known, these formulas can be accurately determined from simple simulated test conditions. The equations of motion of the particles, as derived, are independent of the particle concentration, however they are valid for small particle concentrations which is usually true in gas turbine practical applications.

The effect of flow parameters such as particle mean diameter, particle material density, initial nondimensional particle velocity, and initial gas velocity on the particle trajectories and velocities are discussed.

The calculation of the energy lost due to impacts and the frequency of impacts at each location on the blade surface are important factors in creating an erosion model of the blades. This information can be determined using the results of this study, and correlated with experimental erosion test data can be used as a helpful means to design turbomachine blades for optimum erosion as well as aerodynamic characteristics.

The study of particle trajectories in stationary flow fields in pipes and nozzles have been reported in many articles, such as References 1, 2 and 3. However, none of these investigations take into consideration the collision of particles with the wall or the cascade type flow. In Reference 4 an experimental study was made by the authors to determine the dynamic behavior of solid particles in stationary cascades. The patterns of their trajectories and velocities were the same as predicted by the present study. The locations of the blade surface subjected to severe erosion as determined from this study, agrees with the physical observations of erosion tests made on cascades and real engine stators. The study may have an application for any gas turbine operating with particulated gas flow or any other type of two-dimensional particle suspension.

Equations of Motion of Solid Particles Entrained by the Gas Flow

Drag force on a spherical particle moving in a stream of gas:

Consider the motion of a spherical particle in a steady, very slowly moving incompressible gas flow (Figure a). The inertia forces can be neglected compared to the viscous forces and, for no body forces, the Navier Stokes equations become,

$$\text{grad } P = \mu_g \nabla^2 (\bar{V}_g) \tag{1}$$

The continuity equation of the gas may be written as

$$\text{div } (\bar{V}_g) = 0 \tag{2}$$

Taking the divergence of both sides of Equation (1) and using Equation (2) gives

$$\text{div grad } P = \nabla \cdot \nabla(P) = \nabla^2(P) = 0 \tag{3}$$

The boundary conditions for solving Equation (3) are:

at the particle surface

$$v_{g_t} = v_{g_n} = 0 \tag{4}$$

at a distance very far from the particle

$$\bar{V}_g = \bar{V}_{g_\infty} \tag{5}$$

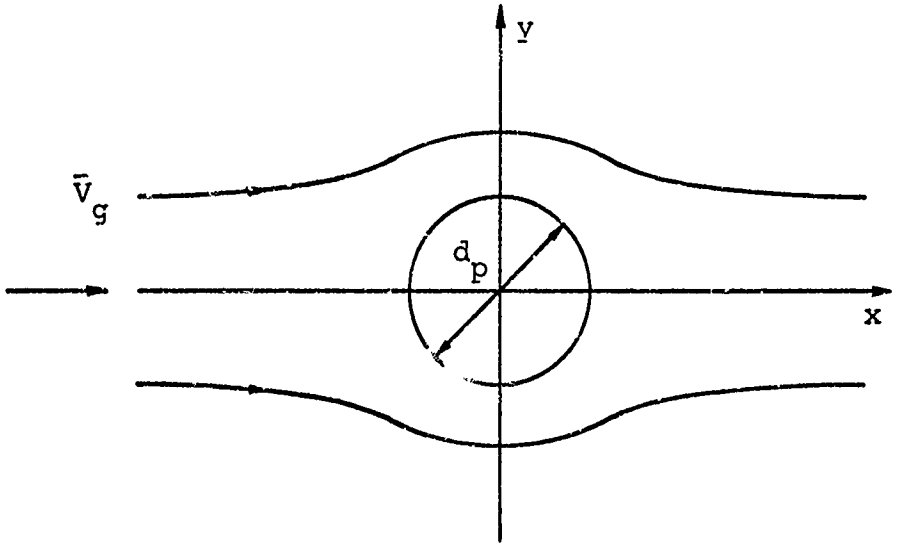

Figure a

From the physical aspects of the problem, and using the boundary conditions, a solution of Equation (3) (Reference 5) gives the pressure on the surface of the sphere as:

$$P = - \frac{6\ \mu_g\ x\ |\bar{V}_{g_\infty}|}{d_p^{\,2}} \tag{6}$$

The velocity components of the gas u_g, v_g and w_g in the x, y and z directions can be determined from Equation (2)(Reference 5). These velocity components are:

$$u_g = |\bar{V}_{g_\infty}|\ [\frac{3}{8}\frac{d_p\ x^2}{r^3}\ (\frac{d_p^{\,2}}{4r^2} - 1) + 1 - \frac{1}{8}\frac{d_p}{r}(3 + \frac{d_p^{\,2}}{4r^2})]$$

$$v_g = |\bar{V}_{g_\infty}| \frac{3}{8} \frac{d_p \, x \, y}{r^3} \left(\frac{d_p^2}{4r^2} - 1\right)$$

$$w_g = |\bar{V}_{g_\infty}| \frac{3}{8} \frac{d_p \, x \, z}{r^3} \left(\frac{d_p^2}{4r^2} - 1\right) \tag{7}$$

where

$$r = \sqrt{x^2 + y^2 + z^2} \tag{8}$$

The shear force can be determined at every point on the surface of the sphere by using the partial derivatives of Equations (7) at the wall. It may be shown that the resultant of the pressure differences relative to the undisturbed flow pressure and the friction forces has the same magnitude at all the points and equals

$$(3 \mu_g |\bar{V}_{g_\infty}|) / d_p$$

Hence, the total drag force acting on the sphere can be determined by multiplying the given resultant force per unit area by the area of the surface of the sphere. This gives

$$\vec{D} = 3 \pi \mu_g d_p \bar{V}_{g_\infty} \tag{9}$$

If the particles are moving with a velocity $\bar{V}_p$ in a stream of gas moving with a velocity $\bar{V}_g$, the whole resistance force on the sphere may be written as,

$$\vec{D} = 3 \pi \mu_g d_p (\bar{V}_g - \bar{V}_p) \tag{10}$$

For higher Reynolds numbers, Equation (10) can not be considered valid, a correction for Equation (10) was then required to allow its use for higher Reynolds numbers. A correction factor which is a function of the Reynolds number was introduced and has different forms depending on the range of the Reynolds number. This correction factor was estimated from experimental results as discussed later. The corrected Equation (10) has the form:

$$\vec{D} = 3 \pi \mu_g d_p (\bar{V}_g - \bar{V}_p) \, g(Re) \tag{11}$$

where

$$g(Re) = C_D \frac{Re}{24}$$

$$\bar{D} = F_i \bar{n}_i = F_x \bar{n}_1 + F_y \bar{n}_2 + F_z \bar{n}_3$$

$$\bar{V}_g = v_{g_i} \bar{n}_i = u_g \bar{n}_1 + v_g \bar{n}_2 + w_g \bar{n}_3$$

$$\equiv \dot{x}_g \bar{n}_1 + \dot{y}_g \bar{n}_2 + \dot{z}_g \bar{n}_3$$

$$\bar{V}_p = v_{p_i} \bar{n}_i = u_p \bar{n}_1 + v_p \bar{n}_2 + w_p \bar{n}_3$$

$$\equiv \dot{x}_p \bar{n}_1 + \dot{y}_p \bar{n}_2 + \dot{z}_p \bar{n}_3 \qquad (12)$$

In Equation (12), $\bar{n}_1$, $\bar{n}_2$ and $\bar{n}_3$ are unit vectors in a frame B in the direction of the mutually perpendicular axes x, y and z respectively. These axes are fixed in an arbitrary blade of the cascade at a point B_o, as shown in Figure b. $\bar{D}$, $\bar{V}_g$ and $\bar{V}_p$ are measured in B. C_D is the drag coefficient on a spherical particle at any Reynolds number.

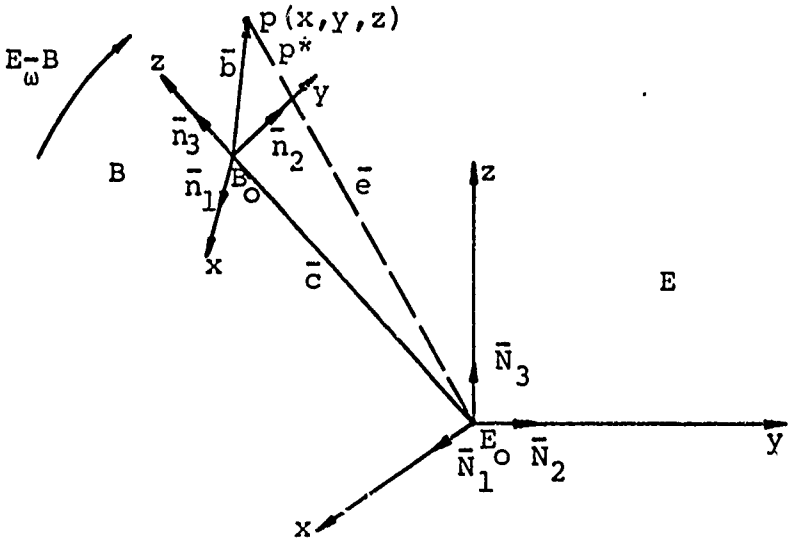

Figure b

Equations of motion of solid particles:

In order to derive the equations of motion of solid particles entrained by gas flow in a cascade, it is convenient to define the following axes systems.

B is a frame fixed in an arbitrary blade of the cascade with $\bar{n}_1$, $\bar{n}_2$ and $\bar{n}_3$ a set of nonparallel, noncoplaner, right handed unit

vectors in the direction of the axes x, y and z, respectively (see Figures b and c). The point B_o, the origin of B, is taken to be the intersection of the plane tangent to the blade row at the entrance and the blade axial chord at the mid-plane that divides the blade height into two equal parts. Further, frame B moves with an angular velocity $\bar{\omega}^{EB}$ in a reference frame E fixed in space. In E, $\bar{N}_1$, $\bar{N}_2$ and $\bar{N}_3$ are unit vectors in the direction of the mutally perpendicular set of axes X, Y, and Z fixed at a point E_o, which is the intersection of the engine axis and a plane normal to it and tangent to the blade row at the entrance.

Consider the motion of a solid particle p in B. Let $\bar{b}$ be the position vector of p relative to B_o, $\bar{e}$ be the position vector of p relative to E_o, and $\bar{c}$ the position vector of B_o relative to E_o (see Figures b and c).

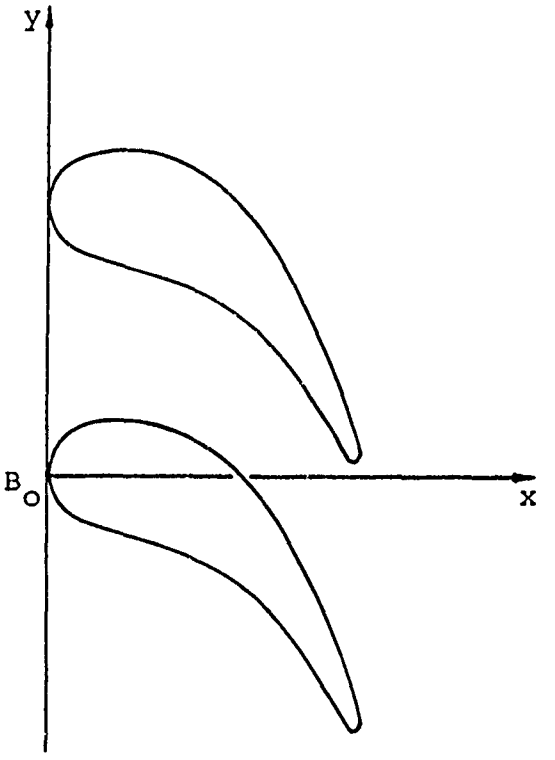

Figure c

Definitions and expressions concerning the motion of a particle in the frame of axes described (Reference 6 and 7) are required to derive the equations of motion of particles.

Referring to Figure b we may write:

1) $\bar{\omega}^{E}_{B}$ is the angular velocity of B in E defined as;

$$\bar{\omega}^{E}_{B} = \dot{\bar{n}}_2 \cdot \bar{n}_3 \, \bar{n}_1 + \dot{\bar{n}}_3 \cdot \bar{n}_1 \, \bar{n}_2 + \dot{\bar{n}}_1 \cdot \bar{n}_2 \, \bar{n}_3 \tag{13}$$

where

$$\dot{\bar{n}}_i = \frac{{}^{E}d\bar{n}_i}{dt} \tag{14}$$

denotes the ordinary derivative of $\bar{n}_i$ with respect to time t in reference frame E.

2) Any vector $\bar{b}$ in B can be written as;

$$\bar{b} = b_i \, \bar{n}_i = b_1 \, \bar{n}_1 + b_2 \, \bar{n}_2 + b_2 \, \bar{n}_3 \tag{15}$$

3) The angular acceleration of B in E is defined as the time derivative in E of the angular velocity of B in E, i.e.;

$$\bar{\alpha}^{E}_{B} = \frac{{}^{E}d(\bar{\omega}^{E}_{B})}{dt} \tag{16}$$

4) For a vector $\bar{b}$ in B which is a function of n scaler variables q_1, q_2, and q_n, we define n first partial derivatives of $\bar{b}$ in B as;

$$\frac{{}^{B}\partial\bar{b}}{\partial q_r} = \sum_{i=1}^{3} \frac{\partial b_i}{\partial q_r} n_i, \qquad r = 1, \quad \cdots\cdots \; n \tag{17}$$

If $\bar{b}$ is only a function of time, the ordinary derivative of $\bar{b}$ with respect to time in B becomes,

$$\frac{{}^{B}d\bar{b}}{dt} = \sum_{i=1}^{3} \frac{db_i}{dt} \bar{n}_i = \frac{db_i}{dt} \bar{n}_i \tag{18}$$

which is true for any vector $\bar{b}$, a function of t in B.

5) Differentiating Equation (15) with respect to t in E, we get;

$$\frac{{}^{E}d\bar{b}}{dt} = \frac{db_i}{dt} \bar{n}_i + b_i \frac{{}^{E}db_i}{dt} \tag{19}$$

Using Equations (13), (14), (15) and (18) in Equation (19), we get;

$$\frac{^{E}d\bar{b}}{dt} = \frac{^{B}d\bar{b}}{dt} + {}^{E}\bar{\omega}^{B} \times \bar{b} \tag{20}$$

6) From Figure b

$$\bar{e} = \bar{c} + \bar{b} \tag{21}$$

Using Equation (20) in Equation (21), the velocity of p in E can be written as;

$$^{E}\bar{V}^{B} = \frac{^{E}d\bar{e}}{dt}$$

$$= \frac{^{E}d\bar{c}}{dt} + \frac{^{E}d\bar{b}}{dt}$$

$$= {}^{E}\bar{V}^{B_o} + \frac{^{B}d\bar{b}}{dt} + {}^{E}\bar{\omega}^{B} \times \bar{b}$$

or

$$^{E}\bar{V}^{p} = {}^{E}\bar{V}^{B_o} + {}^{B}\bar{V}^{p} + {}^{E}\bar{\omega}^{B} \times \bar{b} \tag{22}$$

7) From Figure b, the absolute acceleration of p in E is $^{E}\bar{a}^{p}$, defined as a function of velocity of p in E as;

$$^{E}\bar{a}^{p} = \frac{^{E}d}{dt}\,(^{E}\bar{V}^{p}) \tag{23}$$

The relative acceleration of p in B in terms of the velocity of p in B is

$$^{B}\bar{a}^{p} = \frac{^{B}d}{dt}\,(^{B}\bar{V}^{p}) \tag{24}$$

The absolute acceleration of B_o in E is

$$^{E}\bar{a}^{B_o} = \frac{^{E}d}{dt}\,(^{E}\bar{V}^{B_o}) \tag{25}$$

Substituting Equation (22) into Equation (23), we get,

$$\bar{a}_{EP} = \frac{d}{dt}(\bar{V}_{BO})_E + \frac{d}{dt}(\bar{V}_{BP})_E + [\frac{d}{dt}(\bar{\omega}_B)_E \times \bar{b} + \bar{\omega}_B \times \frac{d\bar{b}}{dt}]_E \quad (26)$$

Using Equations (16), (20) and (25) into Equation (26), we get,

$$\bar{a}_{EP} = \bar{a}_{BO} + [\frac{d}{dt}(\bar{V}_{BP})_E + \bar{\omega}_B \times \bar{V}_{BP}]$$

$$+ \bar{\alpha}_B \times \bar{b} + \bar{\omega}_B \times (\frac{d\bar{b}}{dt})_B + \bar{\omega}_B \times \bar{b}) \quad (27)$$

If B_o was taken to be a point p* coinciding with p, i.e., $\bar{b} = 0$, Equation (27) becomes

$$\bar{a}_{EP} = \bar{a}_{EP^*} + \bar{a}_{BP} + 2\,\bar{\omega}_B \times \bar{V}_{BP} \quad (28)$$

where $\bar{a}_{EP^*}$ is the acceleration in E of a point p* that coincides with p at the instant under consideration.

The equations of motion of a particle moving in a gas stream were derived using Newton's second law of motion, which states that "the absolute acceleration of the particle multiplied by its mass equals the sum of the forces acting on the particle," and may be written as,

$$m_p\,\bar{a}_{EP} = \bar{D} \quad (29)$$

where m_p is the mass of one particle given by:

$$m_p = \frac{\pi d_p^3}{6}\,\bar{\rho}_p \quad (30)$$

Substituting Equations (11), (28) and (30) into Equation (29) we find,

$$\bar{a}_{EP} = \bar{a}_{EP^*} + \bar{a}_{BP} + 2(\bar{\omega}_B \times \bar{V}_{BP})$$

$$= [\frac{18\,\mu_g}{\bar{\rho}_p\, d_p^2}\, g(Re)]\ (\bar{V}_{BG} - \bar{V}_{BP}) \quad (31)$$

Equation (31) describes the motion of a solid particle in a gas stream, it can be further simplified by evaluating the different terms of the equation,

$$\bar{a}^{p^*} = \bar{\alpha}^{B} \times \bar{e} + \bar{\omega}^{B} \times (\bar{\omega}^{B} \times \bar{e})$$

$$= \frac{d}{dt} (-\omega \bar{n}_1) \times \bar{e} + \omega \bar{n}_1 \times \{\omega \bar{n}_1 \times [x_p \bar{n}_1 +$$

$$+ y_p \bar{n}_2 + (z_p + R) \bar{n}_3]\}$$

or

$$\bar{a}^{p^*} = -\omega^2 y_p \bar{n}_2 - \omega^2 (z_p + R) \bar{n}_3 \qquad (32)$$

Also, $\bar{a}^{p}$ is the acceleration of p in B and can be written as,

$$\bar{a}^{p} = \ddot{x}_p \bar{n}_1 + \ddot{y}_p \bar{n}_2 + \ddot{z}_p \bar{n}_3 \qquad (33)$$

Furthermore, the Coriolis acceleration term can be reduced to

$$2(\bar{\omega}^{B} \times \bar{v}^{p}) = 2[(-\omega \bar{n}_1) \times (\dot{x}_p \bar{n}_1 + \dot{y}_p \bar{n}_2 + \dot{z}_p \bar{n}_3)]$$

or

$$2(\bar{\omega}^{B} \times \bar{v}^{p}) = 2\omega \dot{z}_p \bar{n}_2 - 2\omega \dot{y}_p \bar{n}_3 \qquad (34)$$

Substituting Equations (32), (33) and (34) into Equation (31), it reduces to,

$$\ddot{x} \bar{n}_1 + (\ddot{y}_p - \omega^2 y_p + 2\omega \dot{z}_p) \bar{n}_2$$

$$+ [\ddot{z}_p - \omega^2 (z_p + R) - 2\omega \dot{y}_p] \bar{n}_3$$

$$= \left[\frac{18 \mu_g}{\rho_p d_p^2} g(Re)\right][(u_g - u_p)\bar{n}_1 + (v_g - v_p)\bar{n}_2 + (w_g - w_p)\bar{n}_3]$$

(35)

Rearranging Equation (35), letting

$$C = \frac{18\ \mu_g}{\bar{\rho}_p\ d_p^2}\ g(Re) \tag{36}$$

Equation (35) may take the expanded form,

$$\begin{aligned}
\ddot{x}_p &= C\ (u_g - u_p) \\
\ddot{y}_p &= C\ (v_g - v_p) + \omega^2\ y_p - 2\ \omega\ w_p \\
\ddot{z}_p &= C\ (w_g - w_p) + \omega^2\ (z_p + R) + 2\ \omega\ v_p
\end{aligned} \tag{37}$$

In Equation (37), the y distance is measured in a straight line and not a curve which limits the validity of the equations to the case where the radius R of the cascade row is relatively large. In this investigation, concern was focused on the solution of the two-dimensional problem where the motion of gas and particles was considered to be in the x-y plane of a stationary cascade.

It is assumed that,

$$\begin{aligned}
\omega &= 0 \\
w_p &= w_g = 0
\end{aligned} \tag{38}$$

Substituting these assumptions into Equation (37), they simplify to the two equations

$$\ddot{x}_p = C\ (u_g - \dot{x}_p) \tag{39}$$

$$\ddot{y}_p = C\ (v_g - \dot{y}_p) \tag{40}$$

Equations (39) and (40) are the equations of motion of solid particles entrained by the gas flow in a two-dimensional stationary cascade. C is defined by Equation (36) and is a measure of the particle translational characteristic time.

Equations (39) and (40) are two ordinary nonlinear differential equations that can be solved numerically for a given increment of time, to give the x and y coordinates of the particle as well as its velocity components as it passes through the cascade channel. In

order to solve these equations of motion, the following information was required. First, the Reynolds number dependent function g(Re) has to be determined for all practical ranges of application of particulate flow in turbomachines. This will give a more accurate estimate of the drag forces exerted on the particles. Secondly, the gas flow properties, mainly the gas velocity components u_g and v_g and the density ρ_g, have to be known at all points in the flow field for certain flow conditions. Finally, the restitution ratio and the rebound to incidence angle ratio has to be estimated for certain particle target material combinations, which allows the continuation of the solution of Equations (39) and (40) after the particle impact with the wall and its rebound from it. This required information is discussed later in the text and is used in the solution of Equations (39) and (40) for the example cases of a turbine stator and compressor guide vanes which are given in this report.

Drag coefficient for spherical particles:

For a spherical particle moving in a stream of gas the corrected formula for the drag force on the sphere is given by Equation (11), which is

$$\bar{D} = 3\, \mu_g\, \pi\, d_p\, (\bar{V}_g - \bar{V}_p)\, g(Re) \tag{41}$$

In Equation (41) the Reynolds number dependent function g(Re) has different forms depending on the range of the Reynolds number. It should have a value of one for Reynolds numbers less than 1.0. Its value can be determined theoretically from the solution of the Navier Stokes equations for Reynolds numbers up to 4. The experimental data for drag coefficients on a sphere has to be used to determine g(Re) for Reynolds numbers greater than 4 and within the practical limit of Reynolds number for particulate gas flow in turbomachines.

From Equation (10) it can be shown that the drag coefficient of a spherical particle at small Reynolds numbers up to 1.0 can be given by

$$C_{D_o} = \frac{24}{Re} \tag{42}$$

where the Reynolds number is defined as

$$Re = \frac{d_p\, \rho_g}{\mu_g}\, |(\bar{V}_g - \bar{V}_p)| \tag{43}$$

The function g(Re) can then be given as a ratio between the drag coefficient at any Reynolds number and the drag coefficient at small Reynolds number, it may take the form,

$$g(Re) = C_D \qquad \frac{Re}{24} = C_D/C_{D_o} \tag{44}$$

The formulas for the drag coefficient of spherical particles as defined in Equation (44) are given below for different ranges of the Reynolds number.

$$C_D = \frac{24}{Re} \qquad 0 < Re \leq 1.0 \tag{45}$$

For the Reynolds number range $1 < Re \leq 4.0$, a solution of the Navier-Stokes equations of motion of a solid particle using a higher order term (Reference 8) gives the drag coefficient as,

$$C_D = \frac{24}{Re}\left(1 + \frac{3}{16} Re\right)$$

$$1.0 < Re \leq 4.0 \tag{46}$$

For Reynolds numbers up to 2000, the experimental data of Reference 9 for the drag coefficient of spherical particles were fitted and the drag coefficient was given by

$$C_D = 21.9416\ Re^{-0.718} + 0.3240$$

$$4.0 < Re \leq 2000 \tag{47}$$

For higher Reynolds number cases, which are less likely to occur in the problem of gas particle suspension in turbomachines, we may write,

$$C_D = 0.4 \qquad Re > 2000 \tag{48}$$

Detailed discussion of Equations (45) through (48) may be found in Reference 10. These equations, representing the drag coefficient, were used to evaluate the coefficient C in the equations of motion of the solid particles, Equations (39) and (40). Figure 1 gives the fitted drag curve as compared to the experimental results obtained from Reference 9 and it shows very good agreement.

Restitution ratio and rebound to incidence angle ratio for solid particles impinging the blade:

In order to continue the solution of the equations of motion of the particles after the point of collision with the blade, which is a point of discontinuity, it was required to study the impact and rebound phenomena of the particles and blade walls. The value of the particle velocity after rebound and the angle of rebound can be used as initial conditions in the equations of motion after impact.

The particles suffer a loss in momentum due to impact, a decrease in particle velocity and a change of direction. The loss in particle momentum due to collision can be found from the loss in its velocity which was termed restitution ratio. Restitution ratio was defined as the ratio between the particle velocity after and before collision (V_{p_2}/V_{p_1}).

The direction of the particle after it collides with the blade can be determined from the rebound to incidence angle ratio of the particle. This was defined as the ratio of the angle between the direction of the rebound particle velocity and the tangent to the blade surface at the point of impact and the angle between the direction of incoming particle velocity and the tangent to the blade surface at the point of impact (β_2/β_1). This information is enough to define the particle condition after rebound. Since it was very difficult to predict theoretical formulas for these ratios, it was required to determine them empirically and examine their behaviors with the different flow parameters and particle and target materials. Experiments were performed in which the gas particle flow tunnel described in Reference 11 was used to inject particles of different sizes in the flow and photograph their impact with a set of blades fixed at the tunnel's test section.

Particle diameters of 300, 1000 and 2000 microns were used (particle material was corn cups with a density $\bar{\rho}_p = 68.7$ lb/ft^3 and the blades were made of stainless steel). The analysis of the high speed films taken during the runs showed primarily, that the restitution ratio and rebound to incidence angle ratio may be taken as a function of β_1 only. Other parameters seem to have little effect on these ratios. The results of these experiments are shown in Figures 2 through 7. Figure 2 shows that the restitution ratio is independent of the velocity of particle before impact V_{p_1}, decrease in restitution ratio is shown to be mainly due to increase in β_1 as shown from the three curves in Figure 2. Figure 3 shows that the restitution ratio is also independent of the place of collision; the distance x measured in the axial direction for which the gas velocity has different values at the suction as well as pressure sides of the blade. This means that the restitution ratio is not a function of the gas velocity at the point of collision. However, the higher the gas velocity, the higher will be V_{p_1} and hence V_{p_2} will have a higher value, but the ratio V_{p_2}/V_{p_1} is independent of location or gas velocity at impact, again β_1 has the more prominent effect. The data points in the plot of Figures 2 and 3 are for particle diameters 300, 1000 and 2000 microns and they are uniformly distributed along the curves which means that the restitution ratio is independent of the particle diameter. Similar results concerning the independence of V_{p_2}/V_{p_1} on d_p were shown in Reference 12 for particle diameters from 15 to 300 microns.

In Figure 4 the ratio of the particle velocity tangent to the surface after and before collision $(V_{p_{t2}}/V_{p_{t1}})$ were plotted versus

β_1 and may be considered constant for all particle diameters. The dotted line in Figure 4 was used to represent the data on the figure and may be expressed by the equation

$$V_{p_{t2}}/V_{p_{t1}} = 0.95 + 0.00055\ \beta_1 \tag{49}$$

The change in particle velocity due to impact is then mainly due to the contribution of the change in its normal velocity. The change in the ratio between particle velocity normal to the blade surface after and before collision ($V_{p_{n2}}/V_{p_{n1}}$) as a function of β_1 was shown in Figure 5 for different d_p. The dotted curve in Figure 5 represents the data in the figure and may be written as follows:

$$\frac{V_{p_{n2}}}{V_{p_{n1}}} = 1.0 - 0.02108\ \beta_1 + 0.0001417\ \beta_1^2 \tag{50}$$

Equations (49) and (50) are sufficient to define the particle velocity and direction after collision once its velocity in the blade direction and normal to it and its angle of attack were known before the impact. It may be convenient, however, to determine directly curves that give the restitution ratio and the rebound to incidence angle ratio as a function of the incidence angle β_1.

Figure 6 gives β_2/β_1 as a function of β_1 and can be represented by the equation

$$\frac{\beta_2}{\beta_1} = \frac{1}{\beta_1} \cdot \mathrm{Cot}^{-1}\left[\left(\frac{V_{p_{t2}}}{V_{p_{t1}}} \cdot \frac{V_{p_{n1}}}{V_{p_{n2}}}\right) \cdot \mathrm{Cot}\ \beta_1\right] \tag{51}$$

β_2/β_1 has a minimum value at β_1 between 55 and 60°.

In Figure 7 the restitution ratio V_{p_2}/V_{p_1}, is given versus β_1 and it decreases as β_1 increases. The data in Figure 7 may be expressed as,

$$\frac{V_{p_2}}{V_{p_1}} = \frac{V_{p_{n2}}}{V_{p_{n1}}} \cdot \sqrt{\frac{1 + \mathrm{Cot}^2\ \beta_2}{1 + \mathrm{Cot}^2\ \beta_1}} \tag{52}$$

The general trend and order of magnitude of these results may not change much for different target and particle material (results for popy seed particle and plastic blades had practically the same values). Once the particles and blade materials are known, fundamental experiments can render the required information about the impact and rebound phenomena. This information can then be used in

the solution of the equations of motion of particles entrained by gas flow.

Gas flow properties in the cascade channel:

The properties of the gas flow in the cascade is discussed here very briefly. Reference 13 contains a detailed discussion. For nonviscous, irrotational, compressible steady flow in a stationary cascade of a turbomachine the equations of motion are:

1) Combined momentum and continuity equations.

$$\frac{\partial^2\psi}{\partial x^2} + \frac{\partial^2\psi}{\partial y^2} + \left[\frac{\partial(\text{Ln } R)}{\partial x} - \frac{\partial(\text{Ln}[h\rho_g])}{\partial x}\right]\frac{\partial\psi}{\partial x} - \frac{\partial(\text{Ln}[\rho_g])}{\partial y}\frac{\partial\psi}{\partial y} = 0 \tag{53}$$

where

$$u_g = -\frac{1}{h\rho_g}\frac{\partial\psi}{\partial y} \tag{54}$$

$$v_g = \frac{1}{h\rho_g}\frac{\partial\psi}{\partial x} \tag{55}$$

2) Combined state and energy equation.

$$\frac{\rho_g}{\rho_{g_i}} = \left[1 - \frac{v_g^2}{2C_p T_i}\right]^{\frac{\gamma}{\gamma-1}} \tag{56}$$

Boundary conditions for solving Equation (52) are:

a) $\psi = 0$ along 1-4

$\psi = 1$ along 1'-4' (57)

b) Flow along 1-2 and 3-4 are the same as the flow along 1'-2' and 3'-4' respectively and the value of ψ along 1'-2' and 3'-4' is exactly one greater than it is along 1-2 and 3-4.

c) $$\left(\frac{\partial\psi}{\partial x}\right)_i = -\frac{\tan(\beta_i)}{(s\ r)_i} \quad \text{along 1-1'} \tag{58}$$

$$\left(\frac{\partial\psi}{\partial x}\right)_{out} = -\frac{\tan(\beta_{out})}{(s\ r)_{out}} \quad \text{along 4-4'} \tag{59}$$

Figures 8 and 9 show the mesh points in the cascade of a turbine blade and compressor blades respectively. The dimensions of the cascades are given on the respective figures. The computer program given in Reference 14 was modified to give the solution of Equations (53) and (56), that is, the gas velocity in the x and y direction, u_g and v_g, as well as the gas density ρ_g at every mesh point and then store the data on magnetic tapes. These gas properties at the mesh point may be interpolated to give the gas condition at any point in the cascade channel. These values are needed to determine the step by step solution of Equations (39) and (40). Detailed description of the modification of the program of Reference 14 may be found in Reference 15.

Numerical Examples

The dynamic behavior of solid particles suspended by gas flow in the turbine stator and the compressor guide vanes shown in Figures 8 and 9, were calculated by solving the equations of motion of the particles, Equations (38) and (39). In order to investigate the effect of the different flow parameters on the particle trajectories and velocities, particle mean diameter was given the values 1000, 200 and 40 microns, the particle material density was taken to be 34, 68.7 and 151 lb/ft^3 and the initial particle to gas velocity varied from 0.15 to 0.6. Calculation of these cases was used to study the effect of d_p, ρ_p and V_{p_i}/V_{g_i}, on the particle dynamic behavior. At a distance far upstream from the entrance to the turbine or compressor stators, the inlet gas flow conditions were gas inlet velocity V_{g_i} = 142.64 ft/sec in the axial direction, the gas density ρ_{g_i} = 0.076 lb/ft^3 and the gas inlet total temperature T_{g_o} = 60°F. Gas flow properties, ρ_g, u_g and v_g at every mesh point were computed using the modified program of Reference 14. The compressor stator case requires more computer time than the turbine stator case in order for the solution to converge for the same mesh size.

The computer program given by the authors in Reference 15 may be used for the special case of two dimensional particle trajectories to determine the dynamic behaviors of the solid particle in the stators of the turbine and the compressor. The impact and rebound characteristics were described using Equations (51) and (52). The drag coefficient for spherical particles was represented by Equations (45) through (48). The results of this investigation are summarized in the next paragraph.

Turbine stator:

The turbine blading of Figure 8 was used in this study. The airfoil dimensions may be found in Reference 16. The particles were assumed to enter the stator uniformly at a distance one inch

upstream from the blade leading edge. The particle concentration α, (defined as the mass flow rate of particles divided by the mass flow rate of the mixture), specifies the axial and tangential distance between particles, and hence, it determines the place and frequency of collisions, and consequently, the rate at which the blade is eroded. The equations of motion of particles, however, are independent of α. This implies that α can be taken arbitrarily to be any practical value without affecting the reliability of the conclusions of this study.

For easier reference, eleven particles were taken to enter the turbine stator at equal tangential distances apart. Figure 10 shows the trajectories of the eleven particles for d_p = 1000 microns, while Figure 11 shows the corresponding nondimensional velocity distribution of these particles. Similar curves for the trajectories and nondimensional velocities of eleven particles of mean diameters equal 200 and 40 microns are shown in Figures 12, 13, 14 and 15 respectively. The first and the last particles were not taken exactly at the leading edge but slightly shifted in order to determine the direction of motion of the particle after collision. From Figures 10, 12 and 14, which show the particle trajectories for constant ρ_p and V_{p_i}/V_{g_i}, we may observe that, in general, the particles can be divided into three main categories according to their initial place of impact (a manner similar to the conclusions of the experimental results of Reference 4.

The first group of particles are the ones that hit the upper part of the blade leading edge, travel laterally in the nozzle, may or may not hit the opposite blade pressure side, then move outside the nozzle. The second group consists of the particles that hit the pressure side of the blade then leave the nozzle. Finally, the last group of particles are the ones that hit the lower part of the leading edge, travel laterally and may or may not hit the opposite blade suction side or blade pressure side, then move away from the nozzle. It may be interesting to note that, the fact that a particle may or may not hit the opposite blade after hitting the blade leading edge and moving laterally, depends on the pitch, the blade camber and solidity, which are geometrical considerations. Another factor is the mechanism of the impact and rebound phenomena for a certain particle target material combination. Factors that measure the particles path deviation from the gas stream lines are the particle diameter, density and gas and particle velocities. These remarks may be verified by studying Figures 10, 12 and 14, where the three main groups of particles can be easily distinquished. The band width of the particles going out from the stator narrows as the particle diameter decreases, and less impacts were observed, particularly with the blade suction side. From Figures 10, 12 and 14 it may be shown that the areas subjected to erosion are the blade leading edge and pressure sides. (The suction side erosion may be due to particles of higher diameter rejected by the turbine rotor and rebounding back to hit the rear part of the stator's suction side, as may be seen in Reference 17.) The amount of erosion, however, is dependent on the momentum loss due to impacts and the frequency of impacts. Figures 11, 13 and 15 show the nondimensional velocity distribution of the particles given in

Figures 10, 12 and 14, respectively. They show that the particles experience loss in momentum due to collision, the initial rate of increase of the particle velocity is higher for particles of smaller diameter and that the smaller diameter particles attain higher velocities. The particles tend to reach a corresponding constant velocity depending on their respective relaxation time. The distances after which particles tend to approach a certain maximum velocity were of the same order of magnitude (for the given particles it is about 2.5 inches). In discussing the effect of d_p, $\bar{\rho}_p$ and V_{p_i}/V_{g_i} on the particle dynamic behavior a typical particle from each of the three groups of particles were taken as examples and each parameter was allowed to vary separately to predict its influence on the dynamic behavior of the particles.

In order to show the effect of particle mean diameter d_p, on the dynamic behavior, Figures 16, 18 and 20 show the trajectories of the three typical particles for d_p equals 1000, 200 and 40 microns while $\bar{\rho}_p$ and V_{p_i}/V_{g_i} remain constant, Figures 17, 19 and 21 show the nondimensional velocity history of these particles. Figures 16 and 20 show that particles of smaller diameters experience less lateral motion after colliding with the leading edge due to their smaller inertia, as the gas stream tends to force them to decrease their path deviation from gas stream lines, a fact that can also be observed from Figure 18. Figures 17, 19 and 21 indicate that particles with smaller diameters attain higher velocities in the same gas stream, while starting from the same initial velocity. Also, the velocity drop is a function of the respective angle of impact.

The effect of particle material density $\bar{\rho}_p$ on the dynamic behavior of the solid particles for the three typical trajectory type was illustrated by the trajectories of Figures 22, 24 and 26 for $\bar{\rho}_p$ = 34, 68.7 and 151 lb/ft^3, with a constant d_p = 200 microns and a constant V_{p_i}/V_{g_i} = 0.3. Figures 23, 25 and 27 show the corresponding particle nondimensional velocity distribution. These figures show that particles with smaller $\bar{\rho}_p$ have less deviation from the gas stream than those with higher $\bar{\rho}_p$ and that they achieve higher velocities.

The effect of the particle initial nondimensional velocity on the trajectories and velocities for the three particle groups were shown in Figures 28 through 33. Figures 28, 30 and 32 show the particle trajectories for V_{p_i}/V_{g_i} = 0.15, 0.3 and 0.6, a constant d_p = 200 microns and constant $\bar{\rho}_p$ = 68.7 lb/ft^2. Figures 29, 31 and 33 show the velocities of these particles everywhere in the nozzle, nondimensionalized with respect to the initial gas velocity of the free undisturbed stream. The figures show that particle with smaller initial velocity experience less deviation from the gas stream lines due to their smaller inertia. The particles tend to reach the same respective velocity near the end of the nozzle irrespective of their velocity history. In the meantime, higher particle initial velocity relative to the gas corresponds to the case of smaller gas velocity

relative to the particles. Conclusions concerning the effect of initial gas velocity would be that, higher gas initial velocity for particles entering the nozzle with the same speed, density and diameter, will cause the particles to follow more closely the gas stream lines and attain higher velocities. In general, it may be observed that particle mean diameter has more influence on the particle dynamic behavior than the particle material density. On the other hand, the initial particle velocity seems to have smaller effect on the particle behaviors since they tend to reach a constant velocity irrespective of the value of V_{p_i}/V_{g_i}.

Compressor guide vanes:

The compressor blading of Figure 9 is given in detail in Reference 18, as well as the airfoil dimensions. This cascade was used in this investigation. Twelve particles were entered in the nozzle at a distance equals 0.88 inch upstream from the blade leading edge. The trajectories of these particles for d_p = 1000 microns, $\bar{\rho}_p$ = 68.7 lb/ft^3 and V_{p_i}/V_{g_i} = 0.3 are shown in Figure 34. Figures 36 and 38 show the trajectories of similar groups of particles having the same $\bar{\rho}_p$ and V_{p_i}/V_{g_i} and for d_p of 200 and 40 microns, respectively. Figures 35, 37 and 39 show the corresponding non-dimensional velocity distribution. The first and last particles in Figures 34, 36 and 38 were taken slightly above and below the blade leading edge to uniquely define their direction after rebound. Due to the fact that compressor blades have smaller leading edges, the distance between the first two particles and the last two particles of Figures 34, 36 and 38 were taken smaller than the distances between other particles in order to show the groups of particles that hit the blade blunt leading edge. Particles are divided into four groups, the group that initially hit the upper part of the leading edge and move laterally, may or may not hit the opposite blade pressure side then leave the nozzle. The second group are the particles that move without touching the blade surfaces. Because compressor guide vanes have smaller blade thickness and camber than a turbine stator, this group was not observed in the case of a turbine stator. The third group of particles hit the blade pressure side and then leave the nozzle. The final group hit the lower part of the leading edge and move laterally, may or may not hit the opposit blade suction side or blade pressure side, then leave the nozzle. It may be noticed that similar conclusions to that for the turbine stator case can be made for particles moving in compressor guide vanes with one additional observation, that the amount of impact is smaller for the case of compressor stator.

The effect of d_p, $\bar{\rho}_p$ and V_{p_i}/V_{g_i} on the dynamic behavior of the particles moving in a compressor guide vane are similar to the effects for the case of turbine stator. Similar to the case of turbine stator, compressor stator parts that are subjected to more impacts and hence more erosion, are the blade pressure side and leading edge.

CONCLUSION

For a given particle blade material combination, the restitution ratio and rebound to incidence angle ratio may be determined from fundamental test data. The equations of motion of particles entrained by gas flow in a turbine or a compressor stator were solved using the formulas describing the impact and rebound phenomena, proper drag coefficient and gas conditions. The solution of the particle's equations of motion gives the particle trajectories and velocities in the cascade channel. The effect of particle mean diameter d_p, material density $\bar{\rho}_p$ and initial particle and gas velocities on particles dynamic behavior was discussed. A decrease in d_p, $\bar{\rho}_p$ or V_{p_i}/V_{g_i} or increase in initial gas velocity tends to stretch the trajectories in the axial direction. The particle mean diameter has more effect on the particles dynamic behavior than the particle material density. The initial gas and particle velocities have smaller influence. The parts of the blades subjected to the maximum amount of collisions, and hence, erosion damage are the blade leading edge and rear part of the pressure side. For a turbine stator three types of particle trajectories were observed while for compressor guide vanes the same three groups exist plus a group of particles that does not hit the blades at all. The results of this investigation, correlated with experimental erosion tests may be used to design turbomachinery stationary blades for optimum erosion characteristics.

REFERENCES

1. Lapple, C.E. and Shepherd, C.B., "Calculation of Particle Trajectories," Industrial and Engineering Chemistry, Vol. 32, No. 5, May 1940, pp. 605-617.

2. Gilbert, M., Davis, L. and Altman, D., "Velocity Lag of Particles in Linearly Accelerated Combustion Gases," Jet Propulsion, Vol. 25, January 1955, pp. 25-30.

3. Neilson, J.H. and Gilchrist, A., "An Analytical and Experimental Investigation of the Trajectories of Particles Entrained by the Gas Flow in Nozzles," Journal of Fluid Mechanics, Vol. 35, Part 3, 1969, pp. 549-559.

4. Tabakoff, W. and Hussein, M.F., "Trajectories of Particles Suspended in Fluid Flow Through Cascades," AIAA Journal of Aircraft, Vol. 8, No. 1, January 1971.

5. Durand, W.F., "Aerodynamic Theory," Vol. III, Berlin, Julius Springer 1935.

6. Marris, A.W. and Stoneking, C.E., "Advanced Dynamics," McGraw-Hill, Inc., 1967.

7. Kane, T.R., "Dynamics," Hold, Rinhard and Winston, Inc., 1968.

8. Batchelor, G.K., "An Introduction to Fluid Mechanics," Cambridge University Press, 1967.

9. Schlichting, H., "Boundary Layer Theory," McGraw-Hill Inc., 1968.

10. Hussein, M.F. and Tabakoff, W., "Calculation of the Three Dimensional Particle Trajectories in a Compressor Stage, Project Themis Report, University of Cincinnati, Cincinnati, Ohio, to be published.

11. Tabakoff, W. and Hussein, M.F., "Measurements of Particulated Gas Flow Pressure on Cascade Nozzles," AIAA Journal of Aircraft, Vol. 8, No. 2, February 1971.

12. Head, W.J. and Harr, M.E., "The Development of a Model to Predict the Erosion of Material by Natural Contaminant," Wear, An International Journal on the Science and Technology of Friction, Lubrication and Wear Vol. 15, No. 1, January 1970, pp. 1-40.

13. Vavra, M.H., "Aero-Thermodynamics and Flow in Turbomachines," John Wiley and Sons, Inc., 1960.

14. Katsanis, T., "Computer Program for Calculating Velocities and Streamlines on a Blade to Blade Stream Surface of a Turbomachine," NASA-TN D - 4525, April 1968.

15. Hussein, M.F. and Tabakoff, W., "Computer Program to Estimate the Dynamic Characteristics of Solid Particles Entrained by the Gas Flow in a Rotating Cascade of a Turbomachine," Project Themis Report, University of Cincinnati, Cincinnati, Ohio, to be published.

16. Tabakoff, W. and Hussein, M.F., "An Experimental Study of the Effect of Solid Particles in the Pressure at the Blade Surface in Cascade," United States Government Research and Development Report No. AD-703896.

17. Hussein, M.F. and Tabakoff, W., "Calculation of the Three Dimensional Particle Trajectories in a Turbine Stage," Project Themis Report, University of Cincinnati, Cincinnati, Ohio to be published.

18. Emery, J.C., Herring, L.J., Erwin, J.R. and Felix, A.R., "Systematic Two Dimensional Cascade Tests of NACA 65 Series Compressor Blades at Low Speeds," NACA Report No. 1368, 1958.

$$C_D = \frac{24}{Re} \qquad 0 < Re \leq 1.0$$

$$C_D = \frac{24}{Re}\left(1 + \frac{3}{16} Re\right) \qquad 1.0 < Re \leq 4.0$$

$$C_D = (21.9416\, Re^{-0.718} + 0.3246) \qquad 4.0 < Re \leq 2000$$

$$C_D = 0.4 \qquad Re > 2000$$

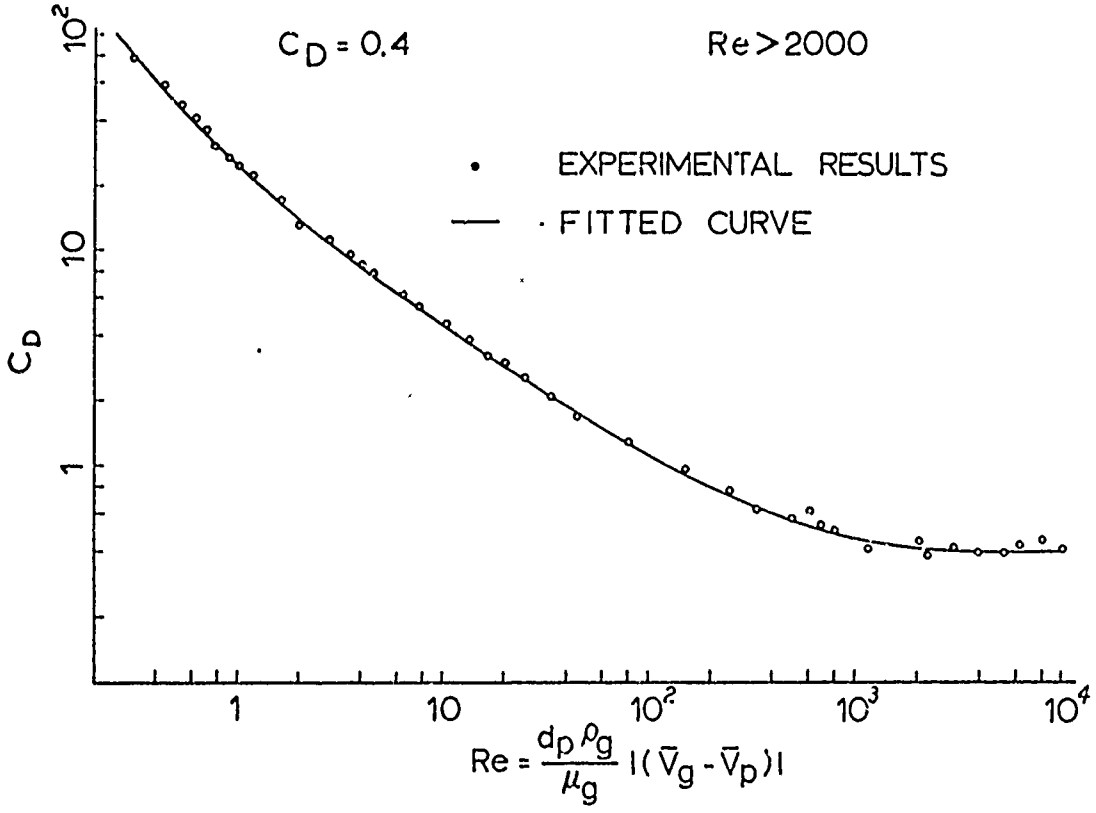

FIG. 1 DRAG COEFFICIENT FOR SPHERICAL PARTICLE

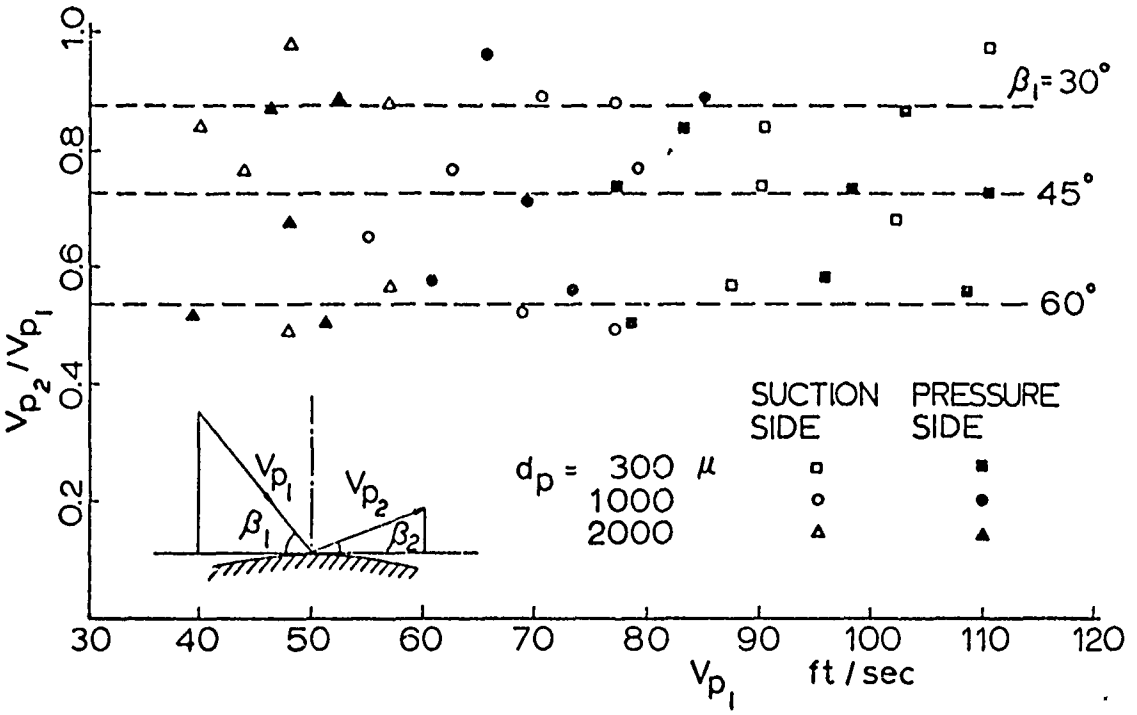

FIG. 2 CHANGE IN RESTITUTION RATIO WITH V_{p_1}

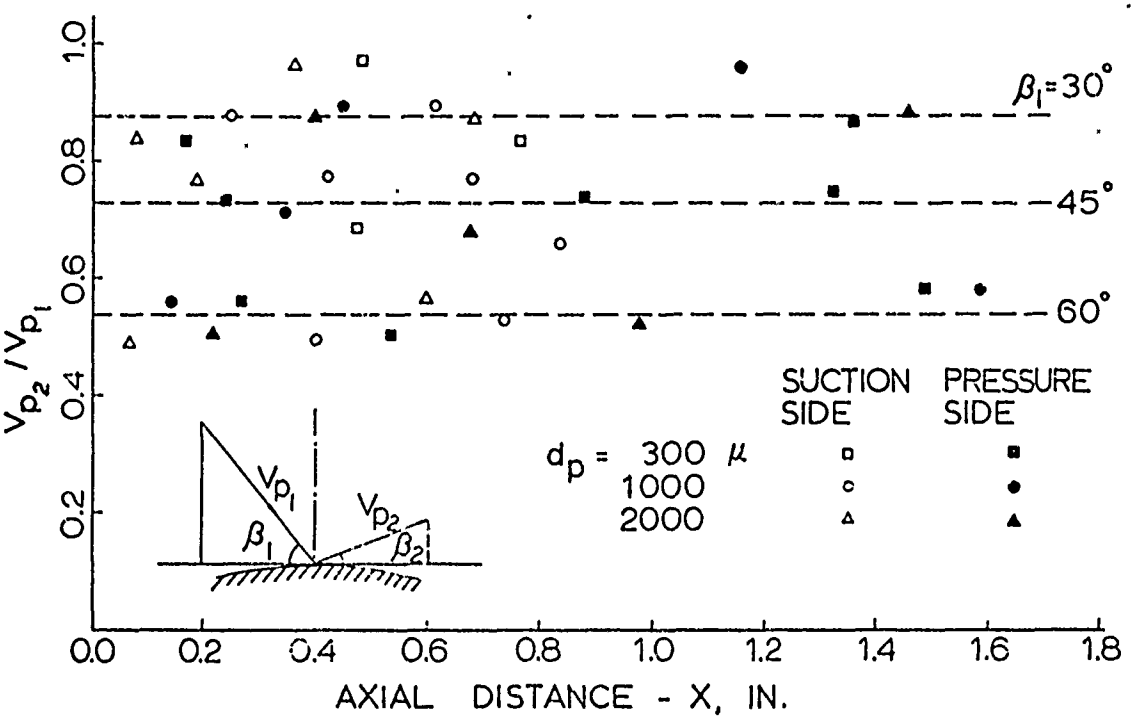

FIG. 3 CHANGE IN RESTITUTION RATIO WITH X

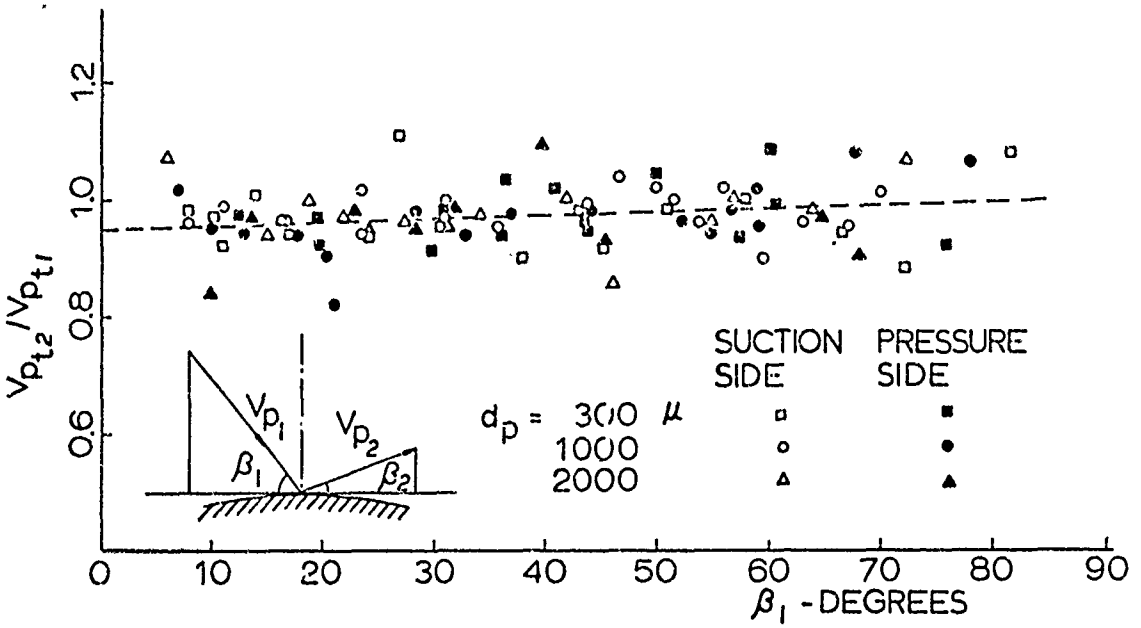

FIG. 4 DROP IN PARTICLE RELATIVE TANGENTIAL VELOCITY DUE TO COLLISION

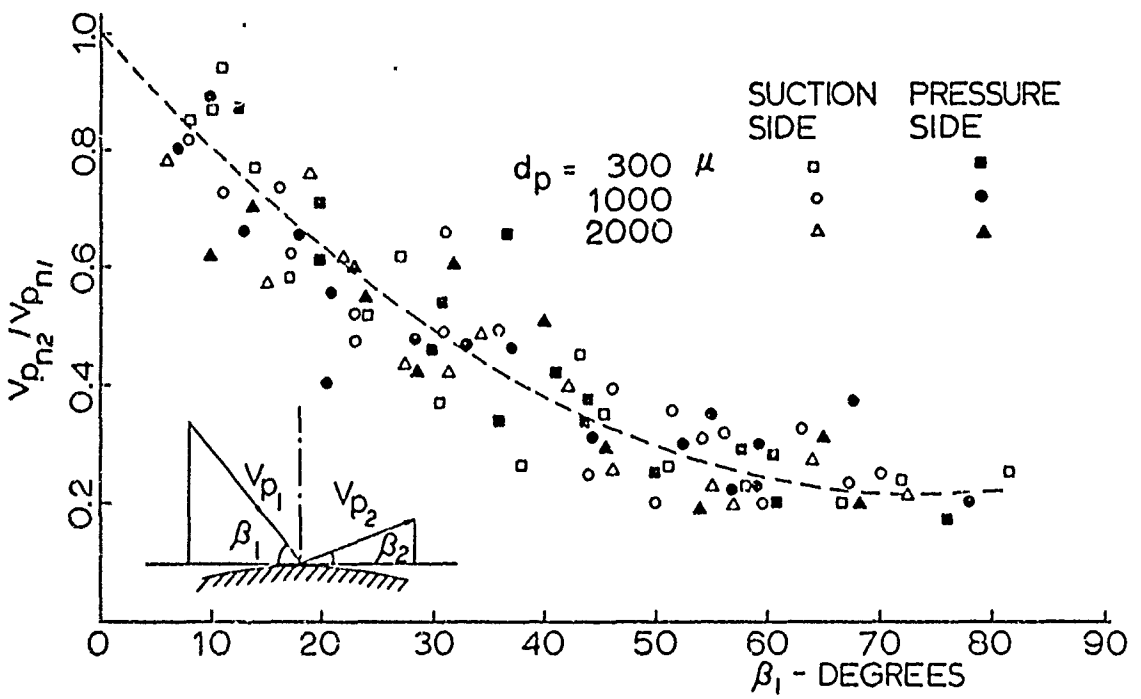

FIG. 5 DROP IN PARTICLE RELATIVE NORMAL VELOCITY DUE TO COLLISION

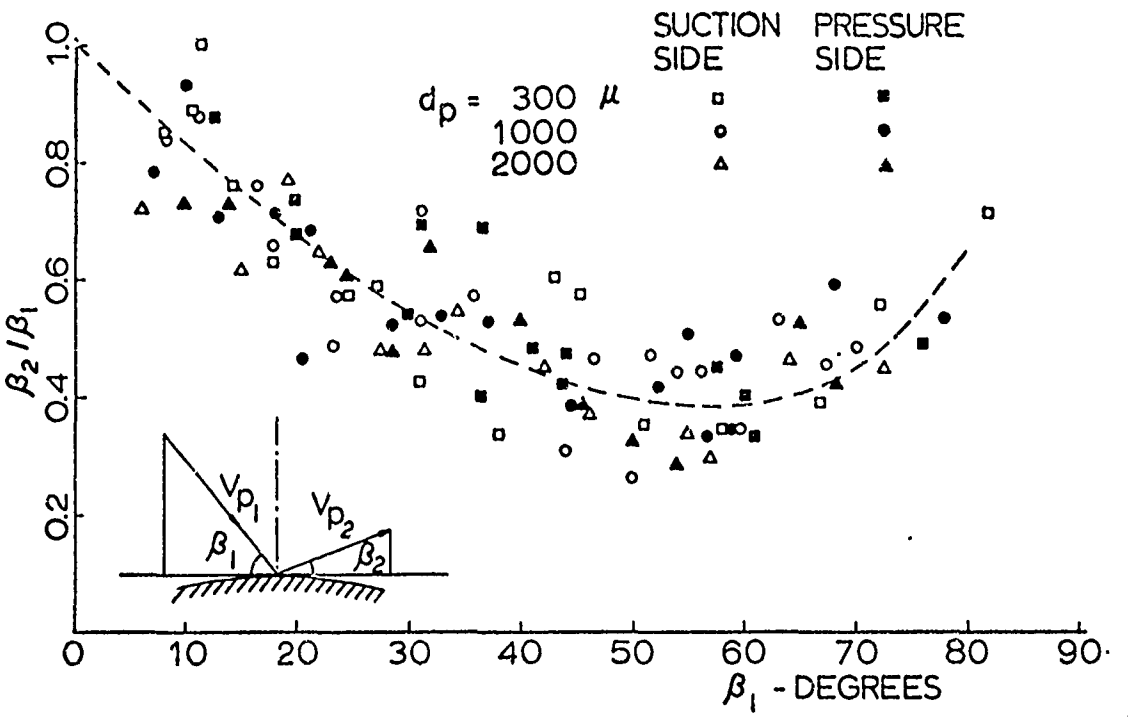

FIG. 6 NONDIMENSIONAL ANGLE OF REBOUND

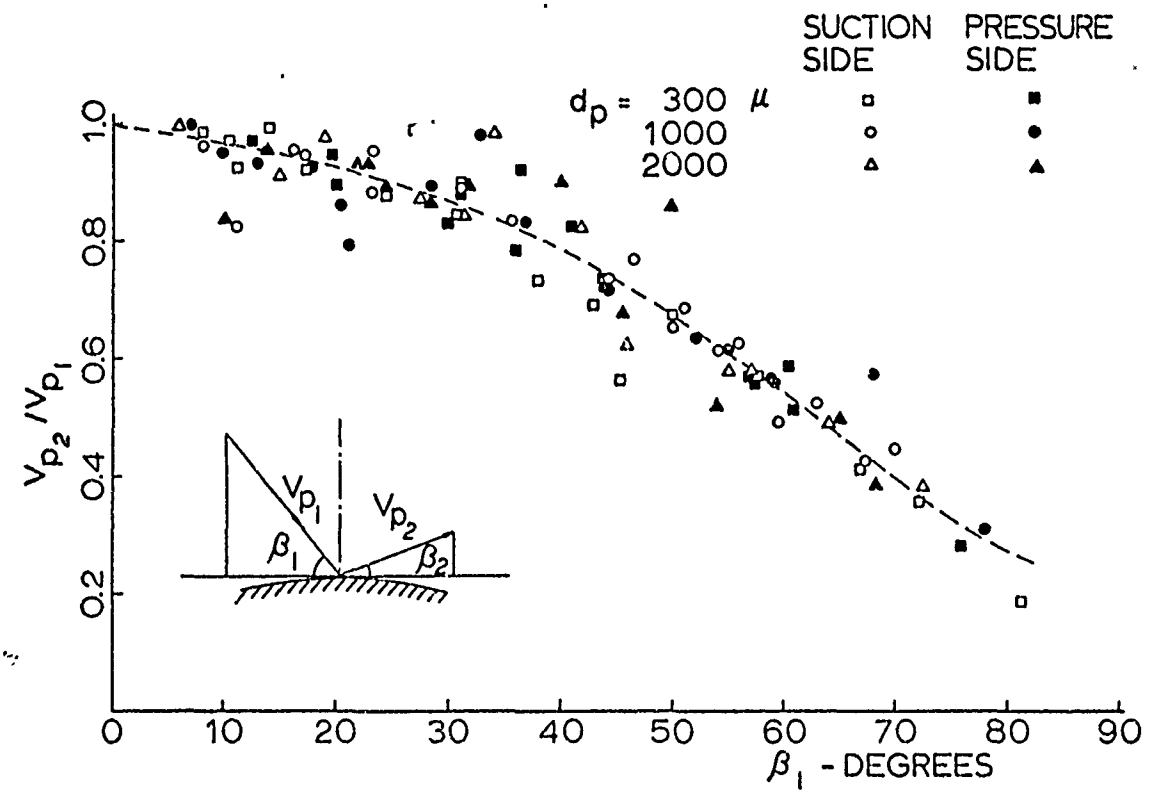

FIG. 7 DROP IN PARTICLE RELATIVE VELOCITY DUE TO COLLISION (RESTITUTION RATIO)

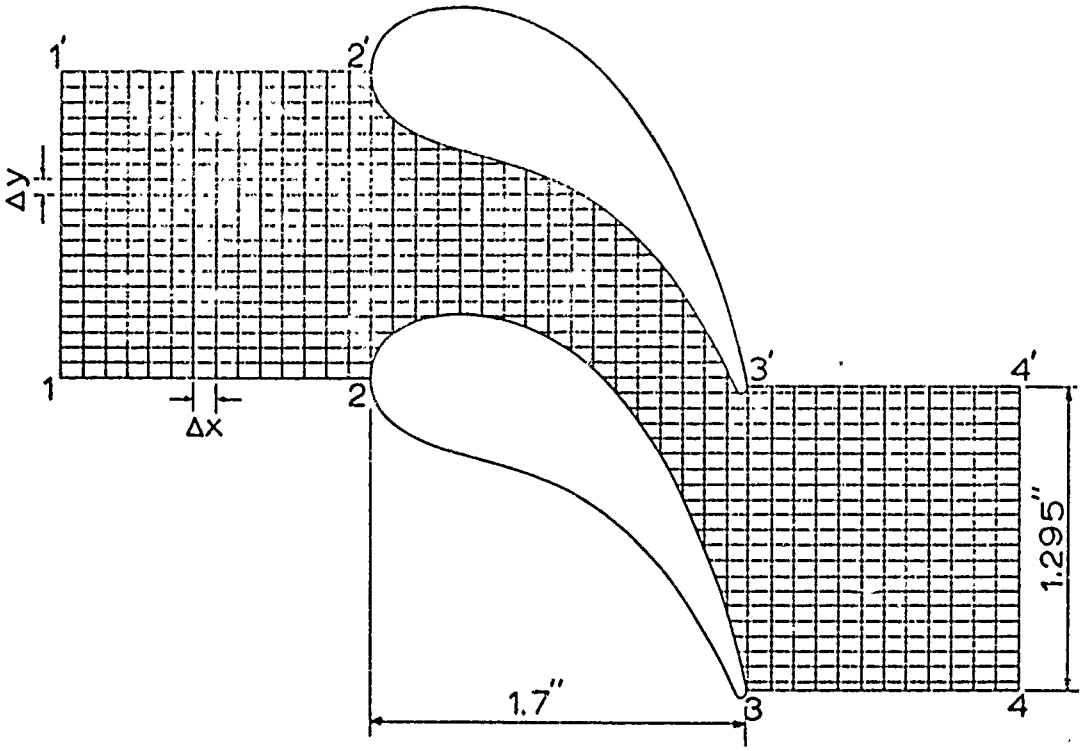

FIG. 8 MESH POINTS FOR TURBINE STATOR

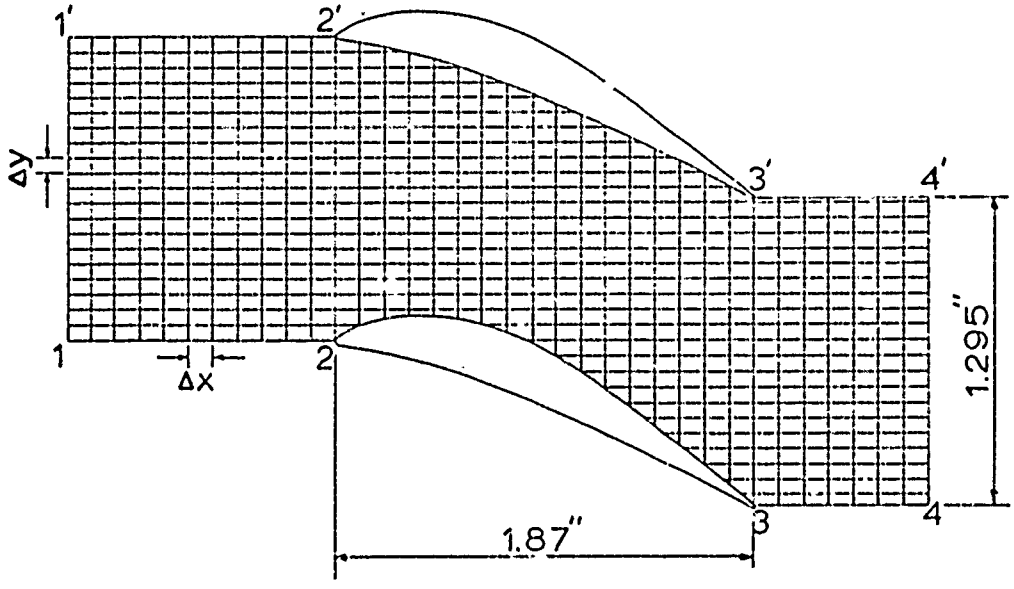

FIG. 9 MESH POINTS FOR COMPRESSOR GUIDE VANE

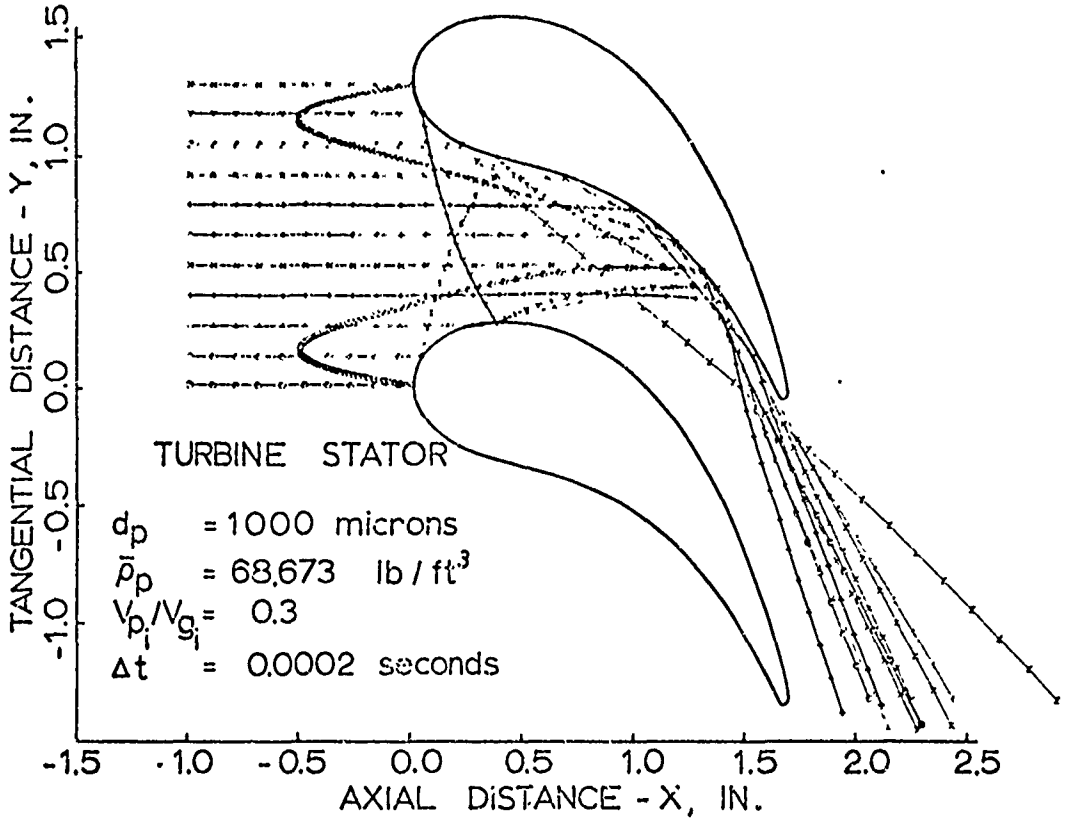

FIG.10 PARTICLE TRAJECTORIES

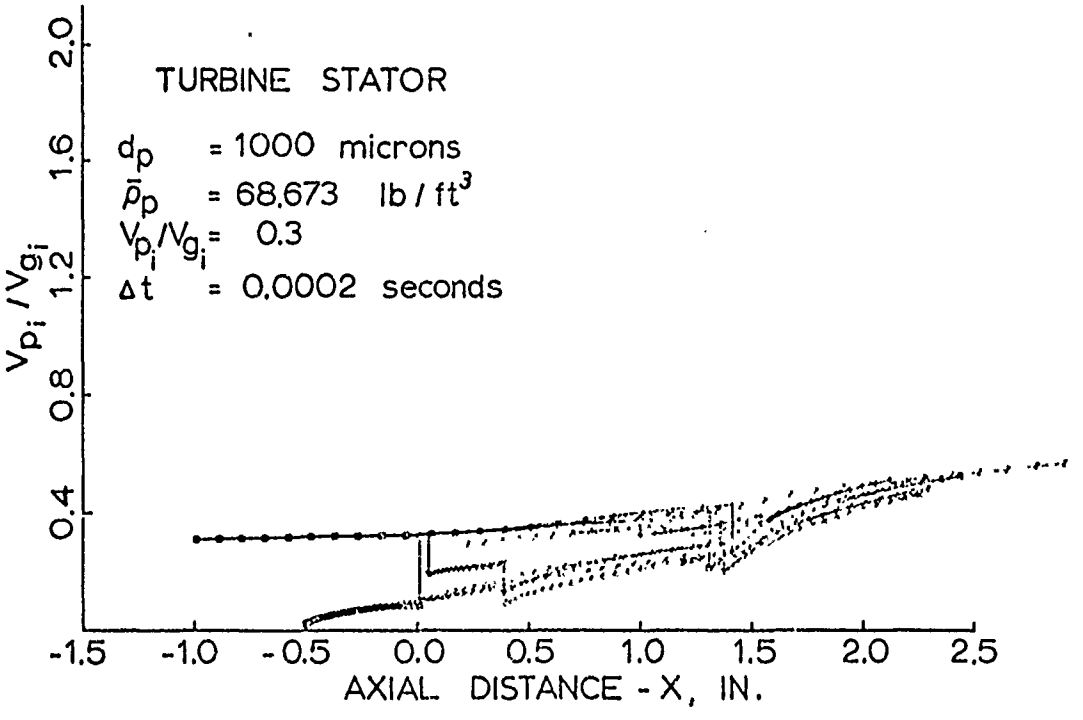

FIG.11 PARTICLE NONDIMENSIONAL ABSOLUTE VELOCITY

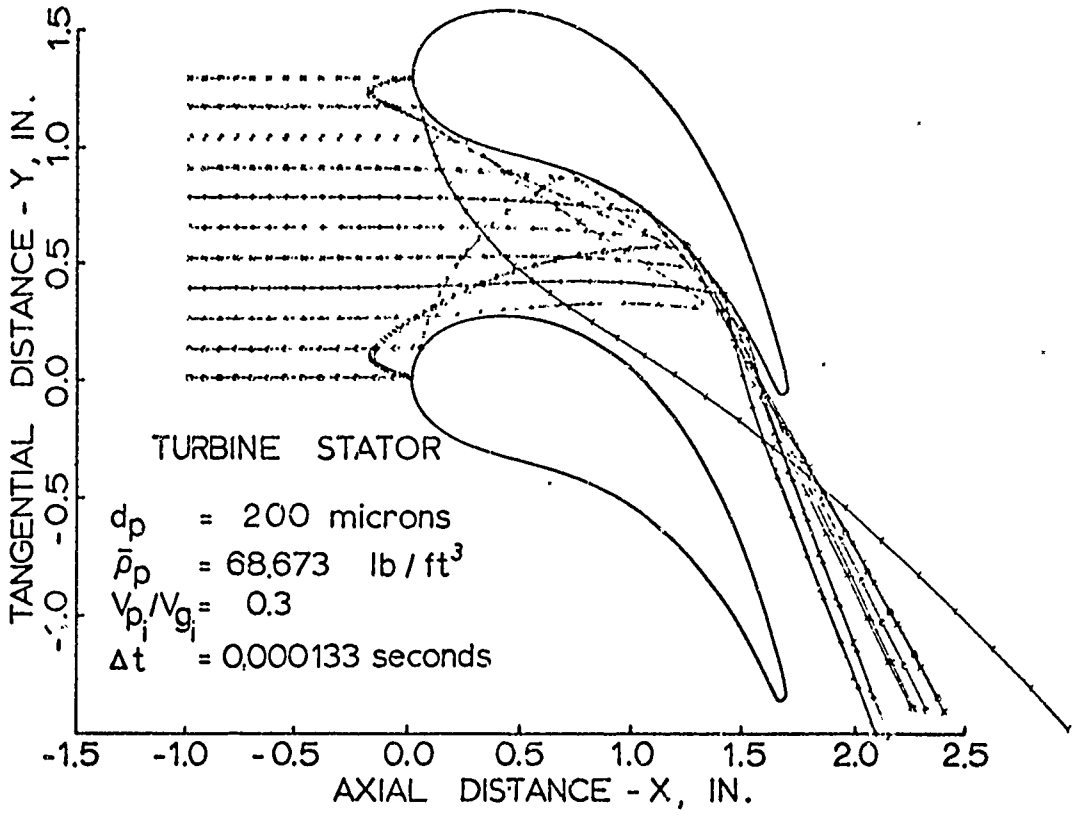

FIG.12 PARTICLE TRAJECTORIES

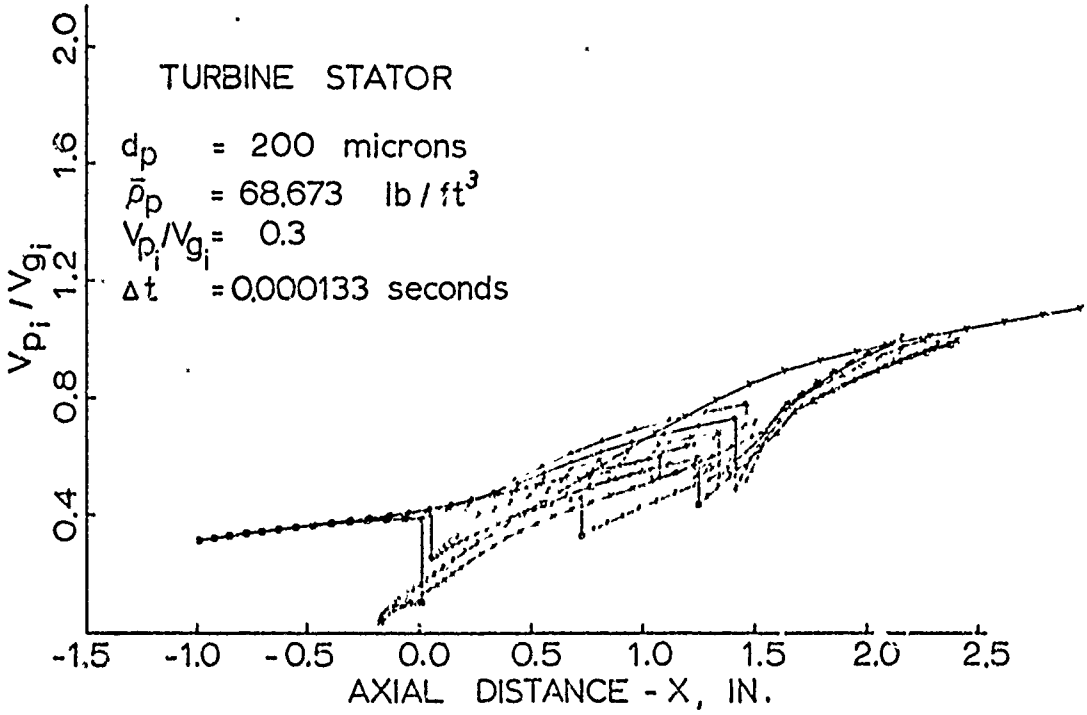

FIG.13 PARTICLE NONDIMENSIONAL ABSOLUTE VELOCITY

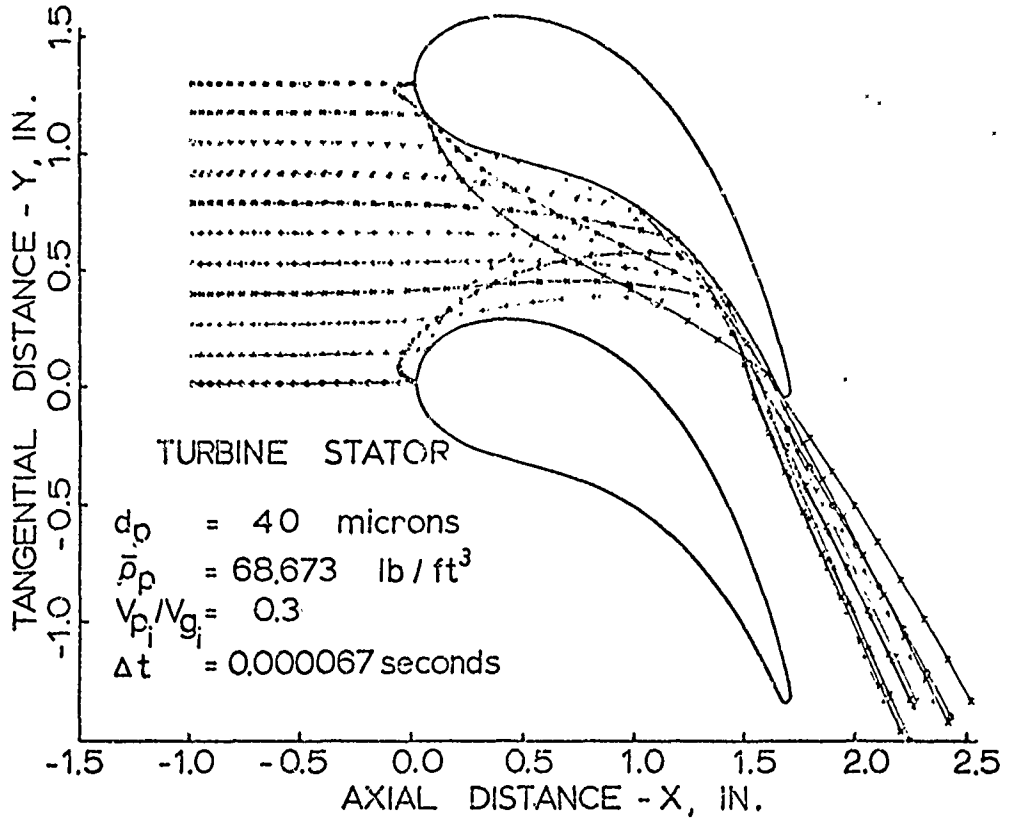

FIG.14 PARTICLE TRAJECTORIES

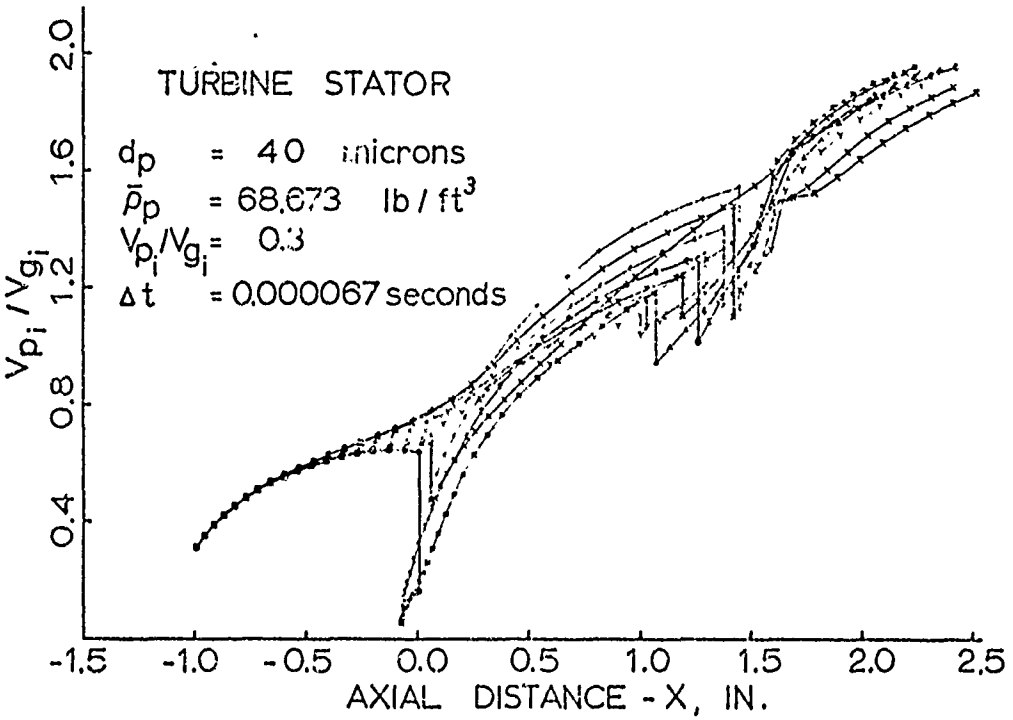

FIG.15 PARTICLE NONDIMENSIONAL ABSOLUTE VELOCITY

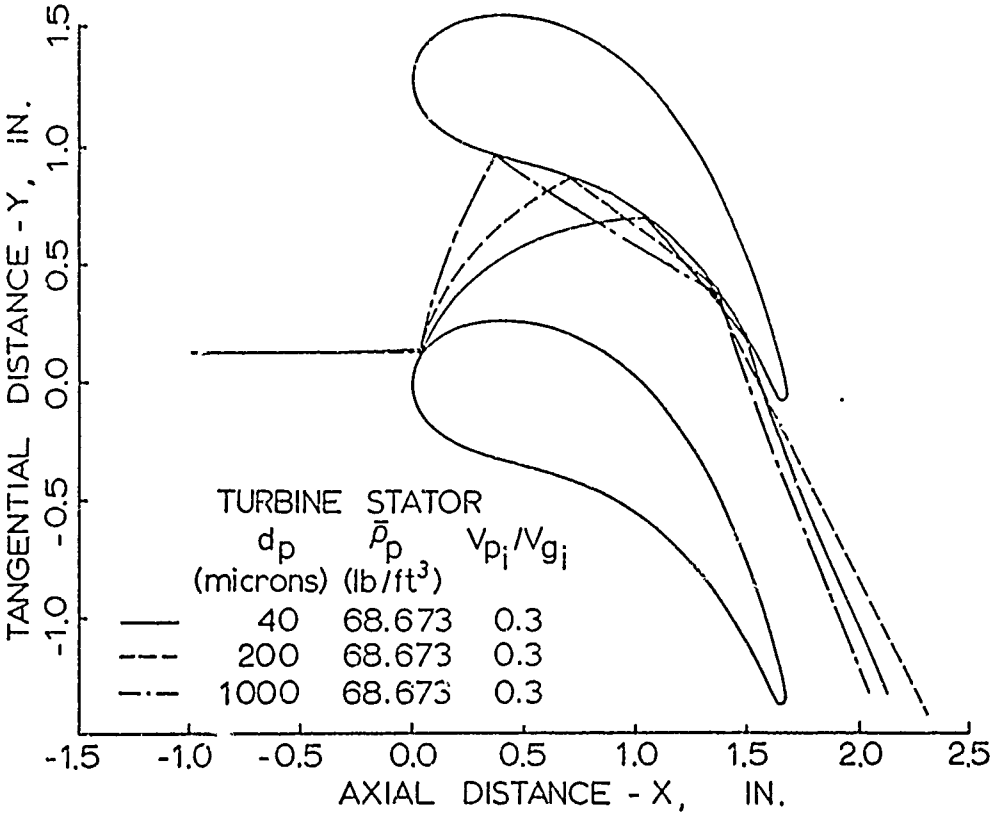

FIG.16 PARTICLE TRAJECTORIES (EFFECT OF d_p)

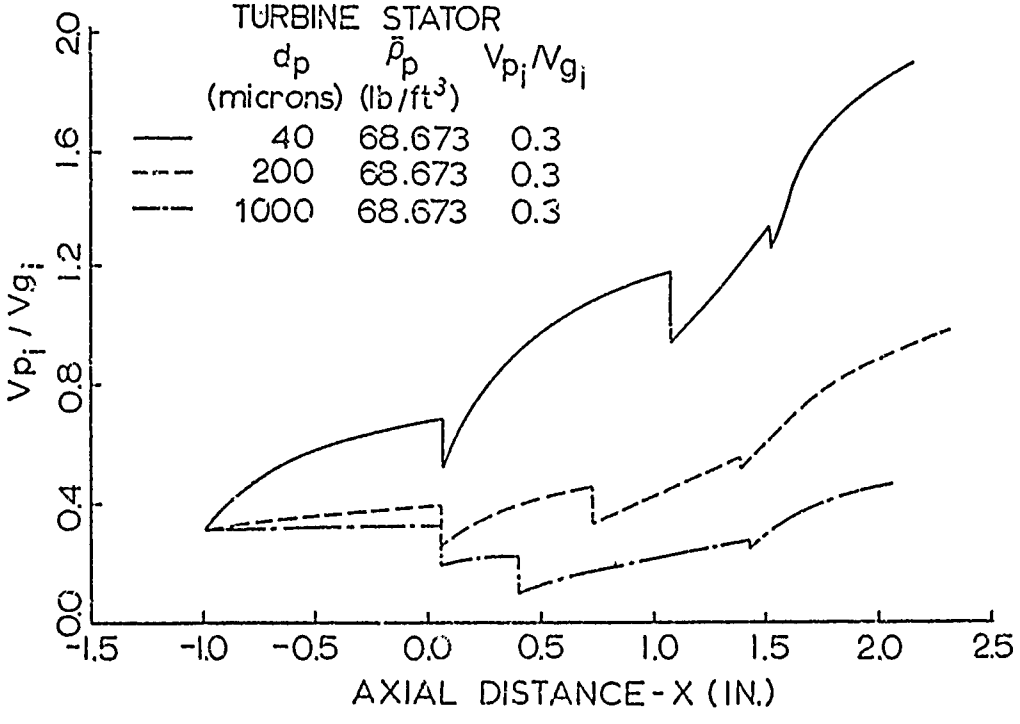

FIG.17 PARTICLE NONDIMENSIONAL ABSOLUTE VELOCITY (EFFECT OF d_p)

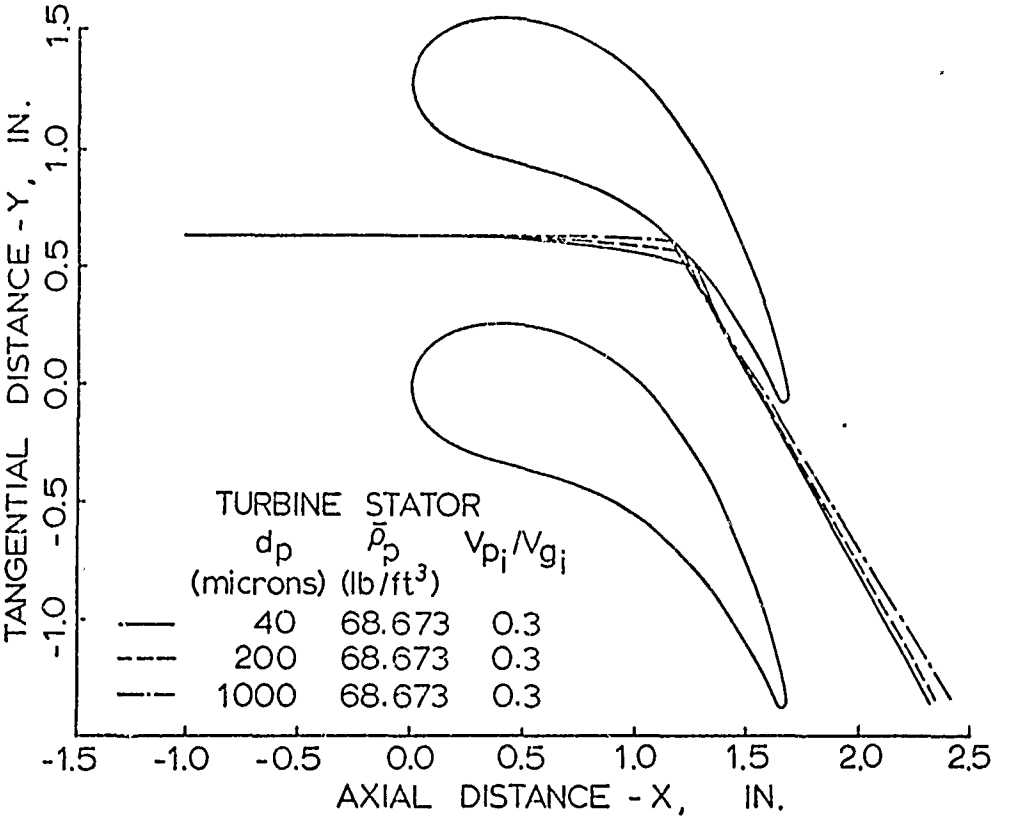

FIG.18 PARTICLE TRAJECTORIES (EFFECT OF d_p)

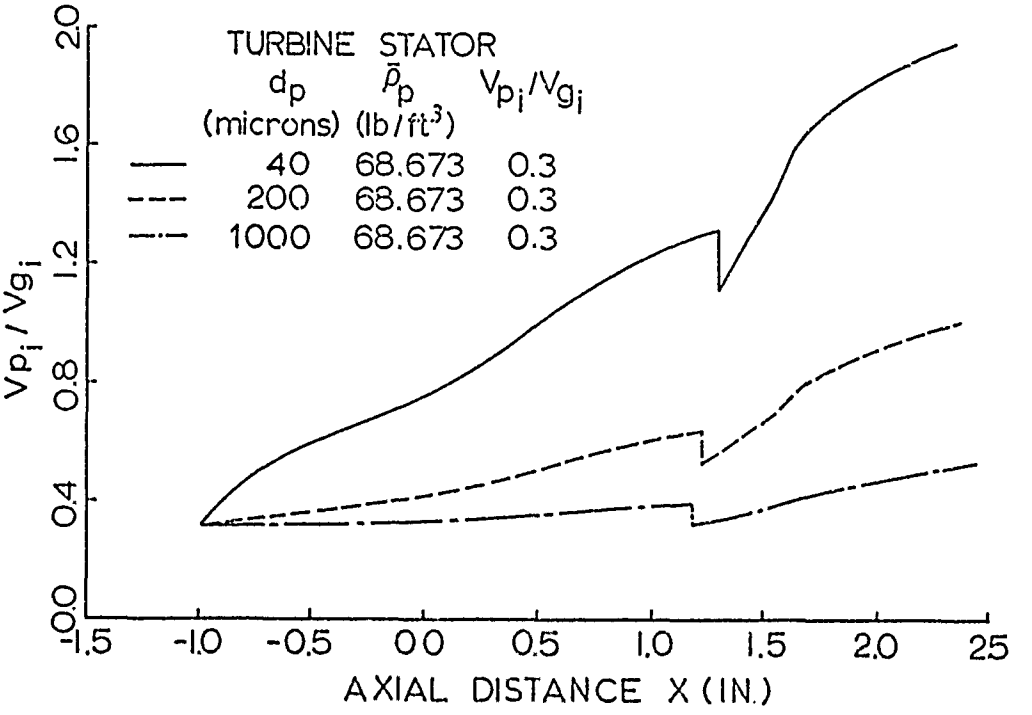

FIG.19 PARTICLE NONDIMENSIONAL ABSOLUTE VELOCITY (EFFECT OF d_p)

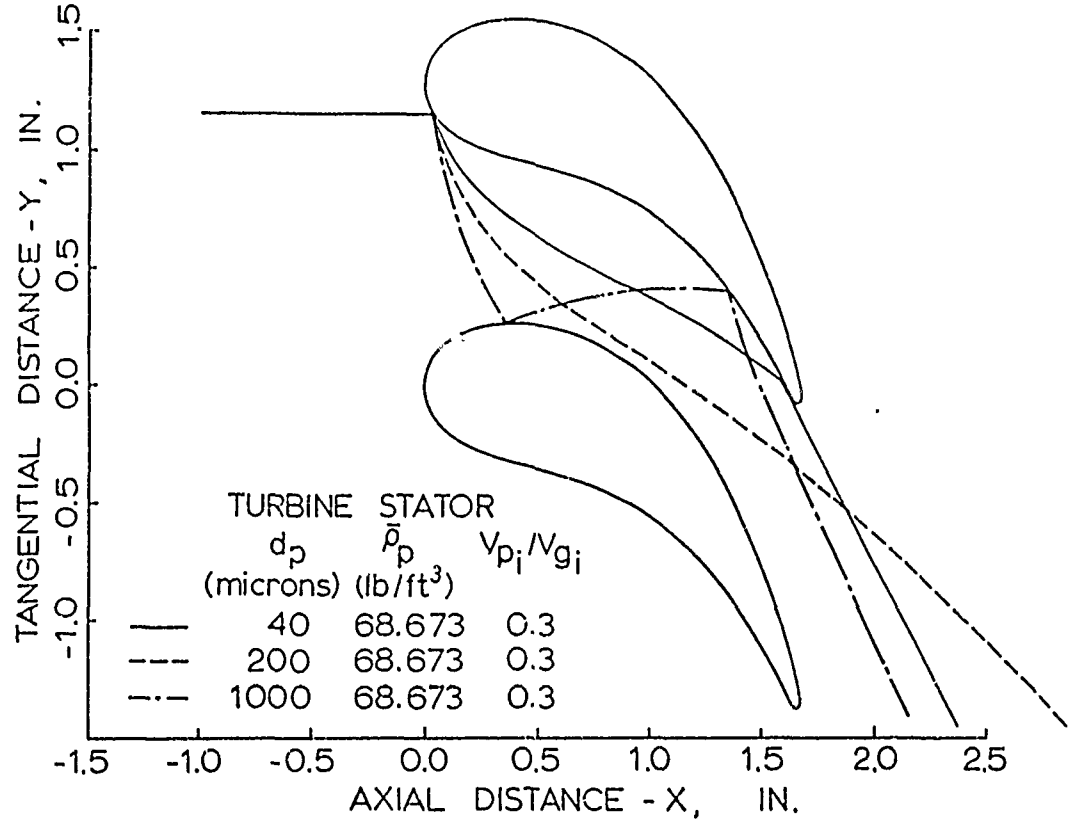

FIG. 20 PARTICLE TRAJECTORIES (EFFECT OF d_p)

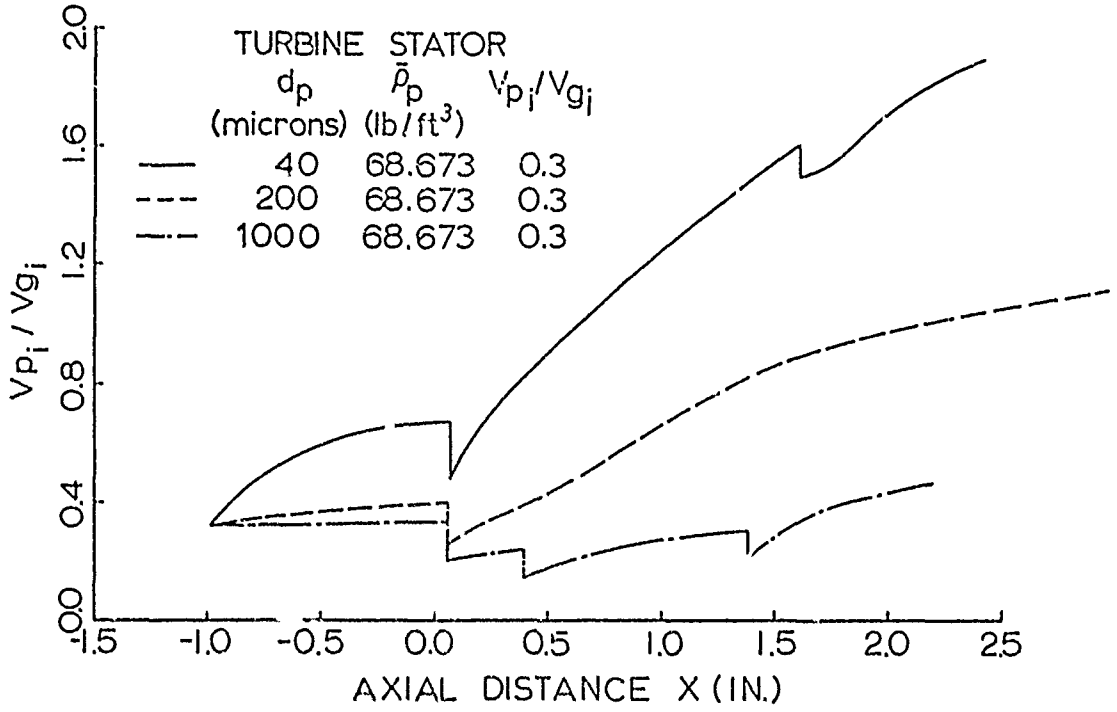

FIG. 21 PARTICLE NONDIMENSIONAL ABSOLUTE VELOCITY (EFFECT OF d_p)

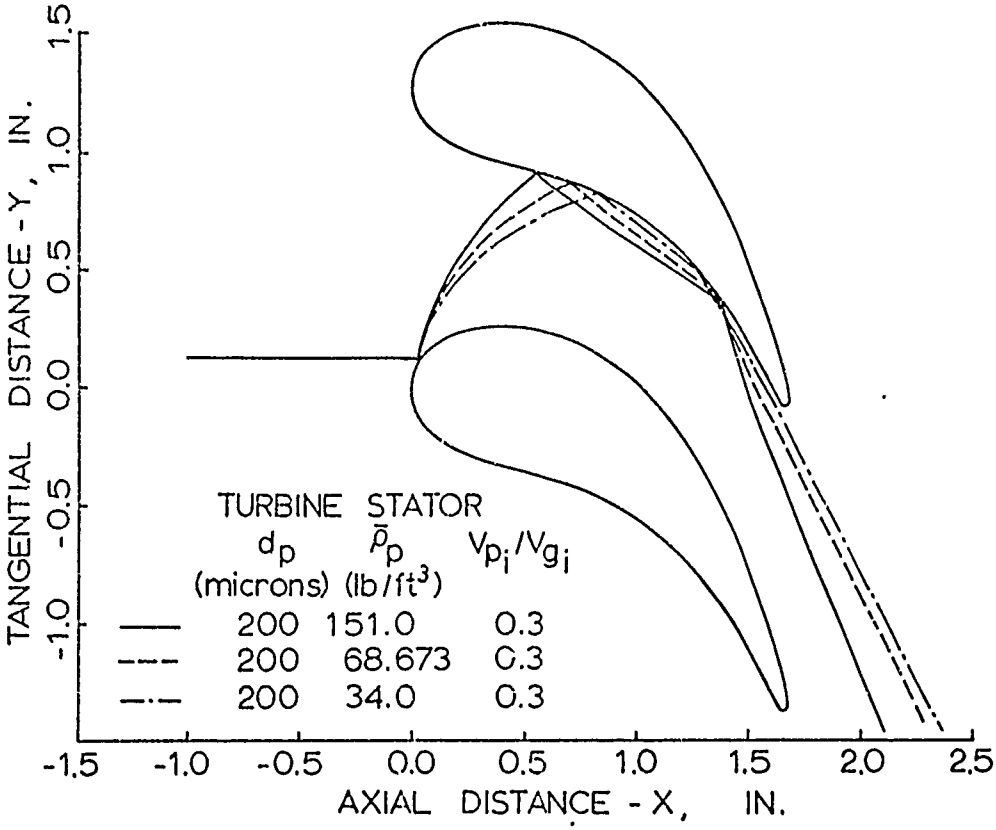

FIG. 22 PARTICLE TRAJECTORIES (EFFECT OF $\bar{\rho}_p$)

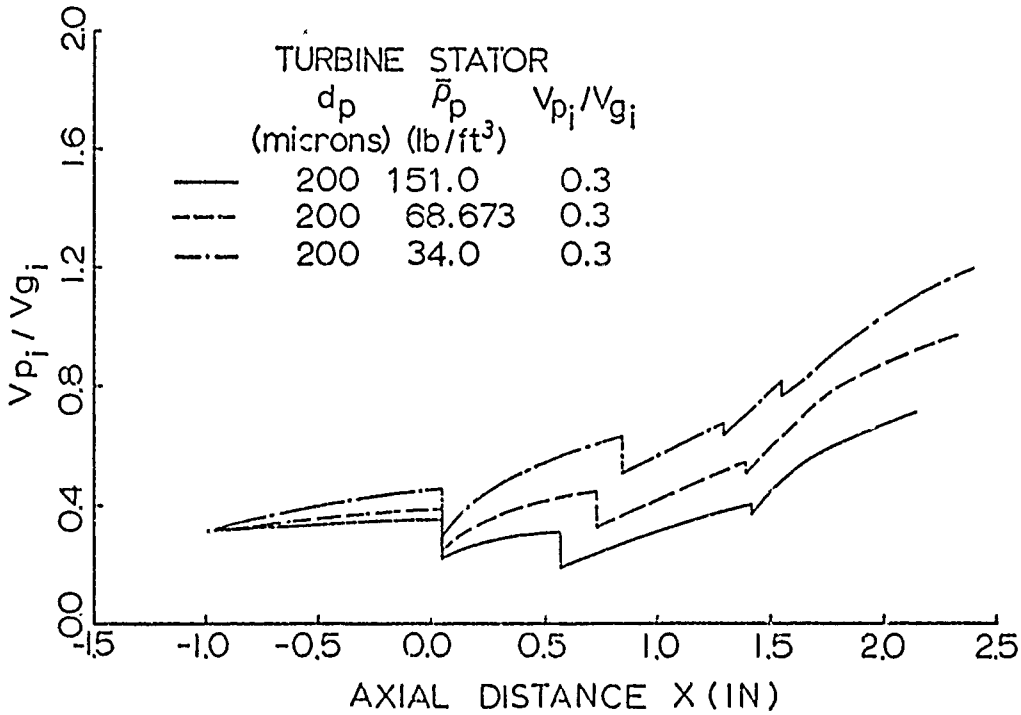

FIG. 23 PARTICLE NONDIMENSIONAL ABSOLUTE VELOCITY (EFFECT OF $\bar{\rho}_p$)

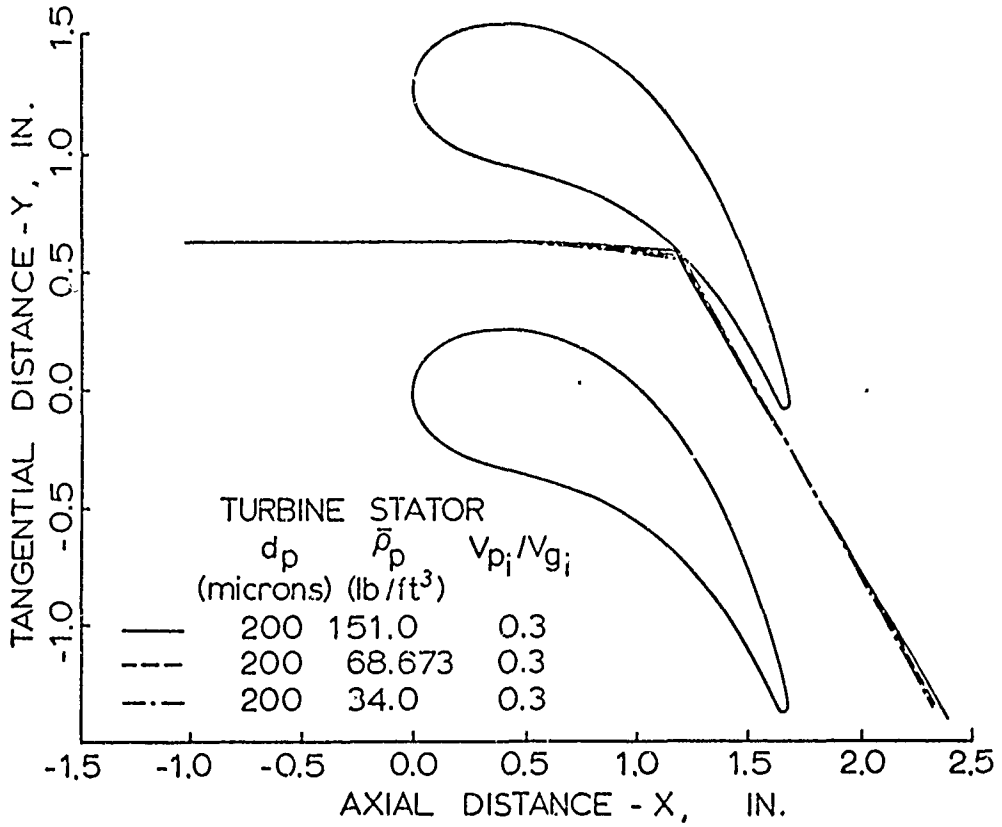

FIG.24 PARTICLE TRAJECTORIES (EFFECT OF $\bar{\rho}_p$)

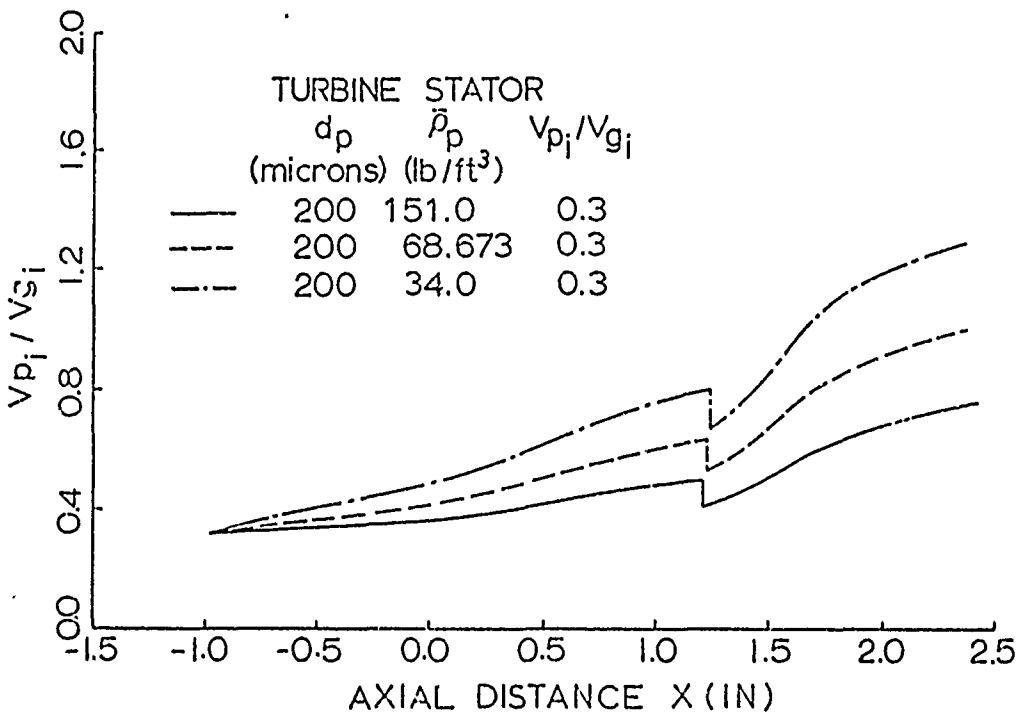

FIG.25 PARTICLE NONDIMENSIONAL ABSOLUTE VELOCITY (EFFECT OF $\bar{\rho}_p$)

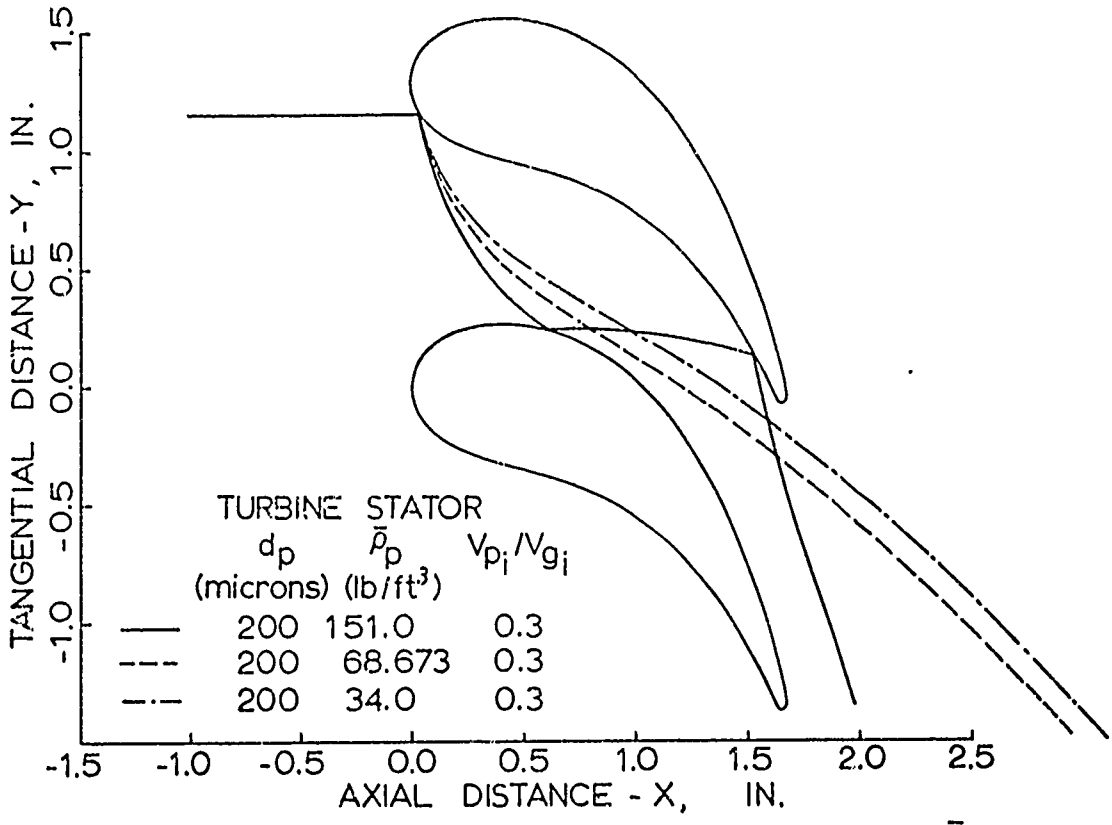

FIG. 26 PARTICLE TRAJECTORIES (EFFECT OF $\bar{\rho}_p$)

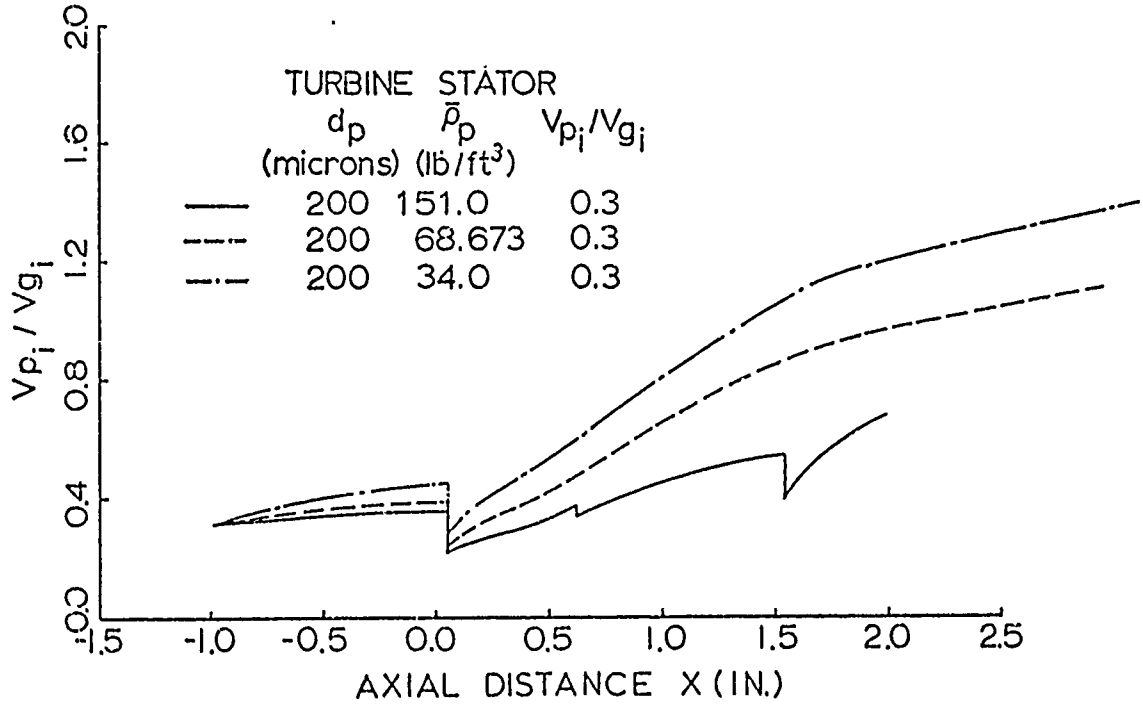

FIG.27 PARTICLE NONDIMENSIONAL ABSOLUTE VELOCITY
(EFFECT OF $\bar{\rho}_p$)

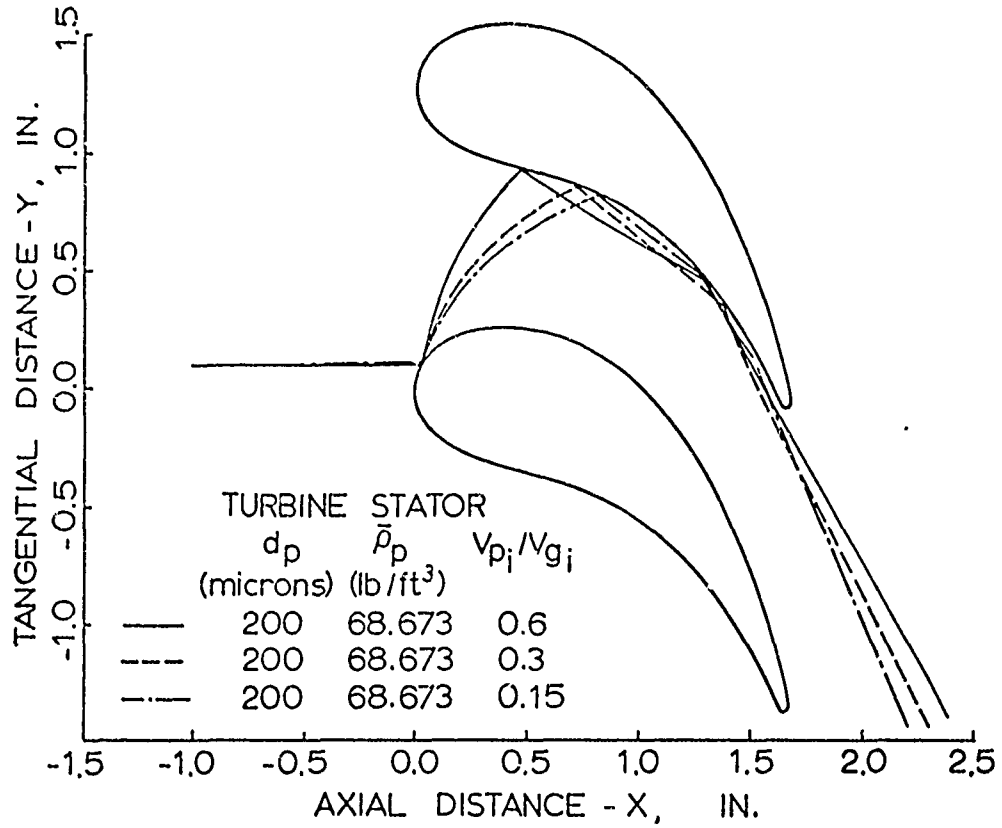

FIG.28 PARTICLE TRAJECTORIES (EFFECT OF V_{p_i}/V_{g_i})

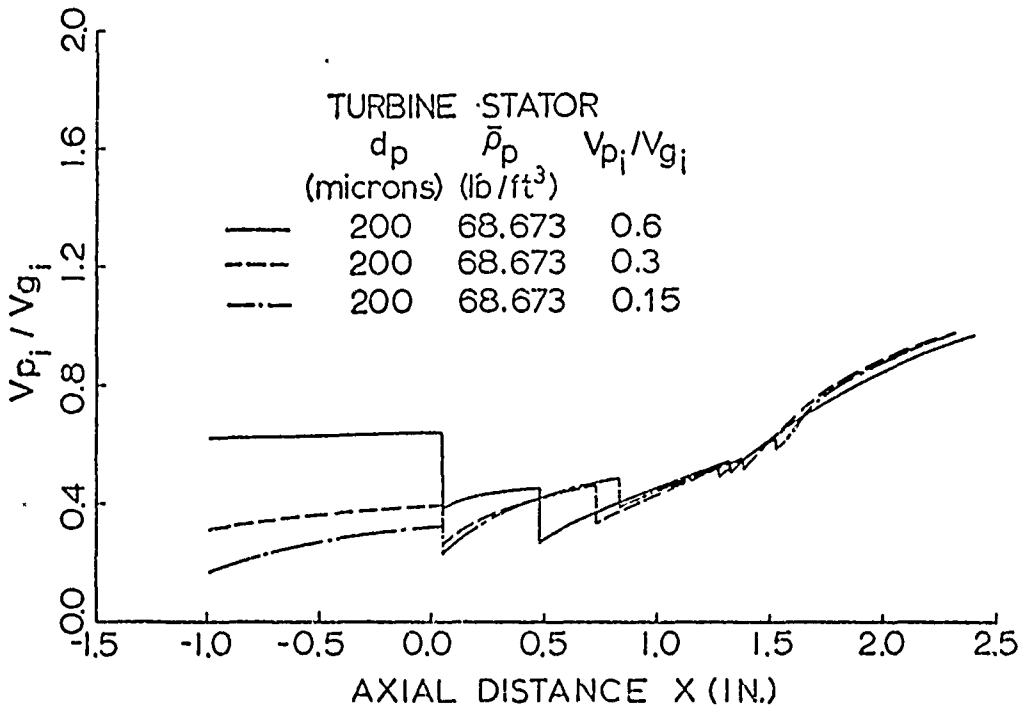

FIG.29 PARTICLE NONDIMENSIONAL ABSOLUTE VELOCITY (EFFECT OF V_{p_i}/V_{g_i})

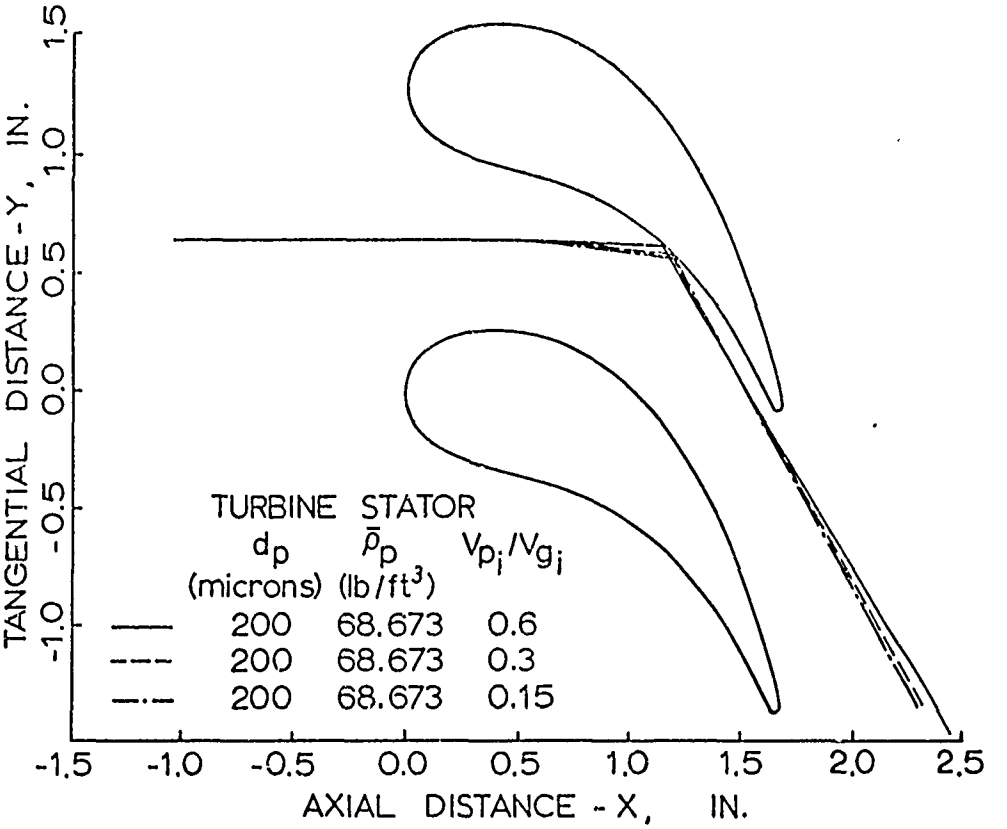

FIG.30 PARTICLE TRAJECTORIES (EFFECT OF V_{p_i}/V_{g_i})

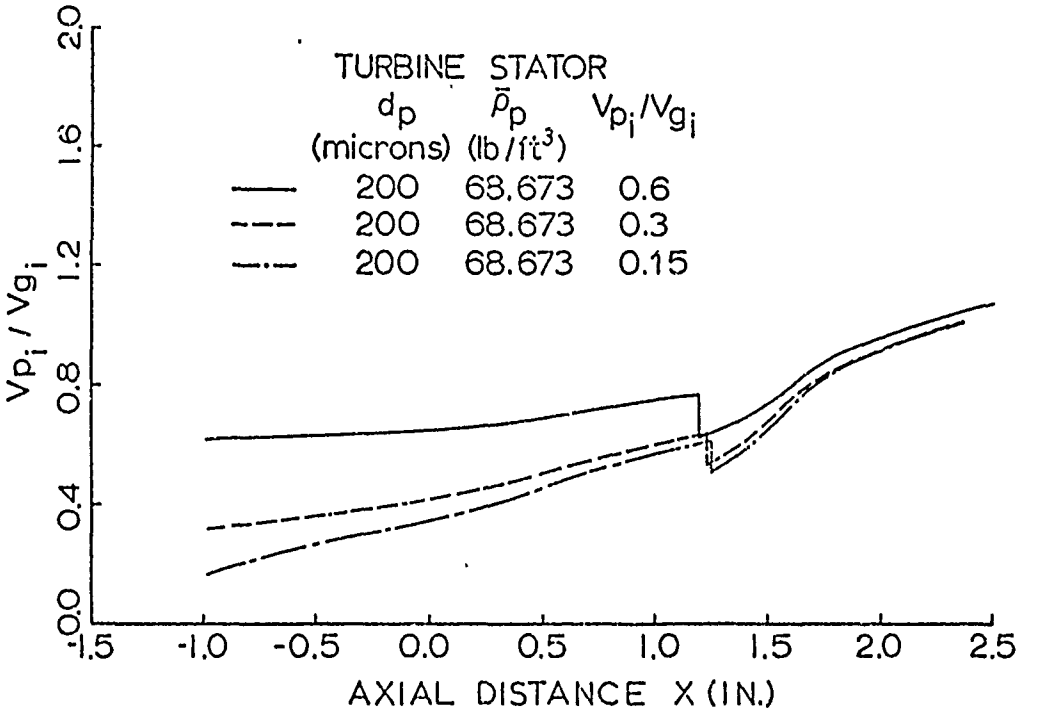

FIG.31 PARTICLE NONDIMENSIONAL ABSOLUTE VELOCITY (EFFECT OF V_{p_i}/V_{g_i})

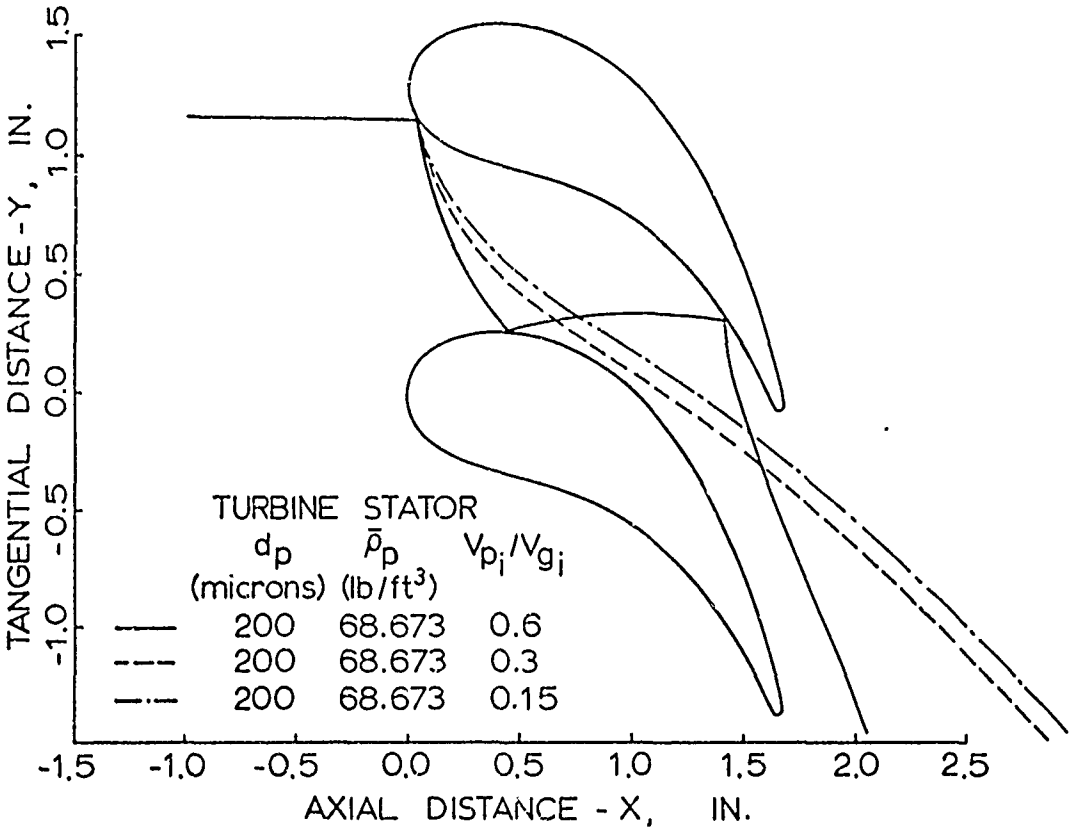

FIG.32 PARTICLE TRAJECTORIES (EFFECT OF V_{p_i}/V_{g_i})

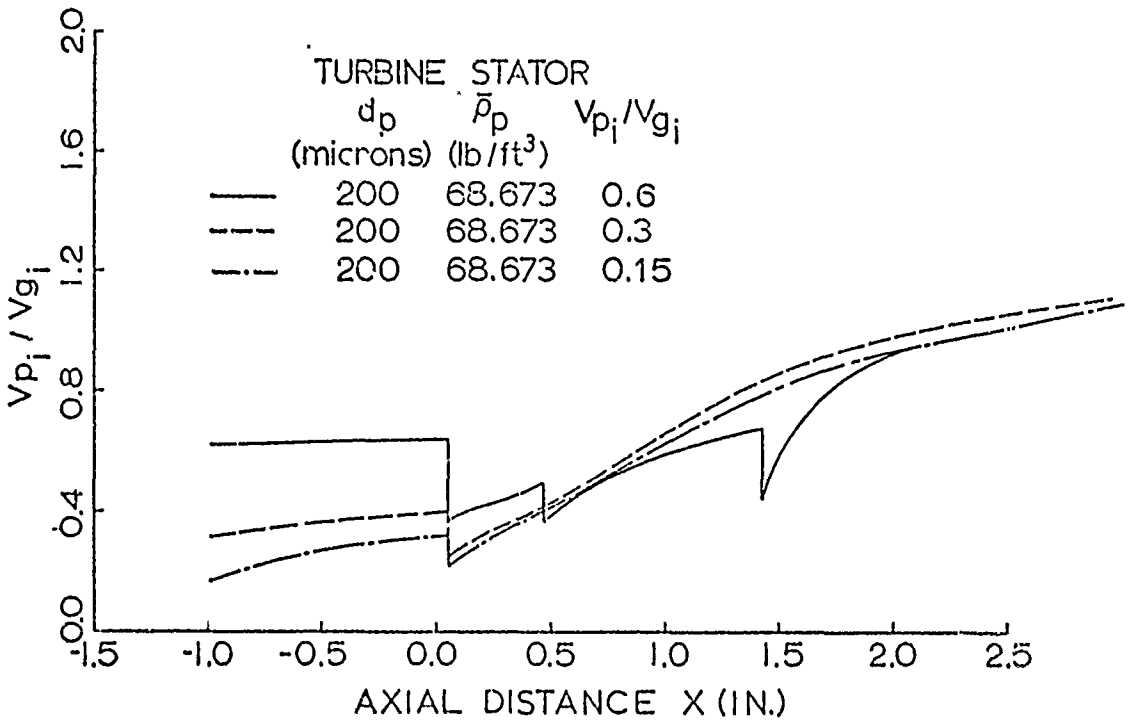

FIG.33 PARTICLE NONDIMENSIONAL ABSOLUTE VELOCITY (EFFECT OF V_{p_i}/V_{g_i})

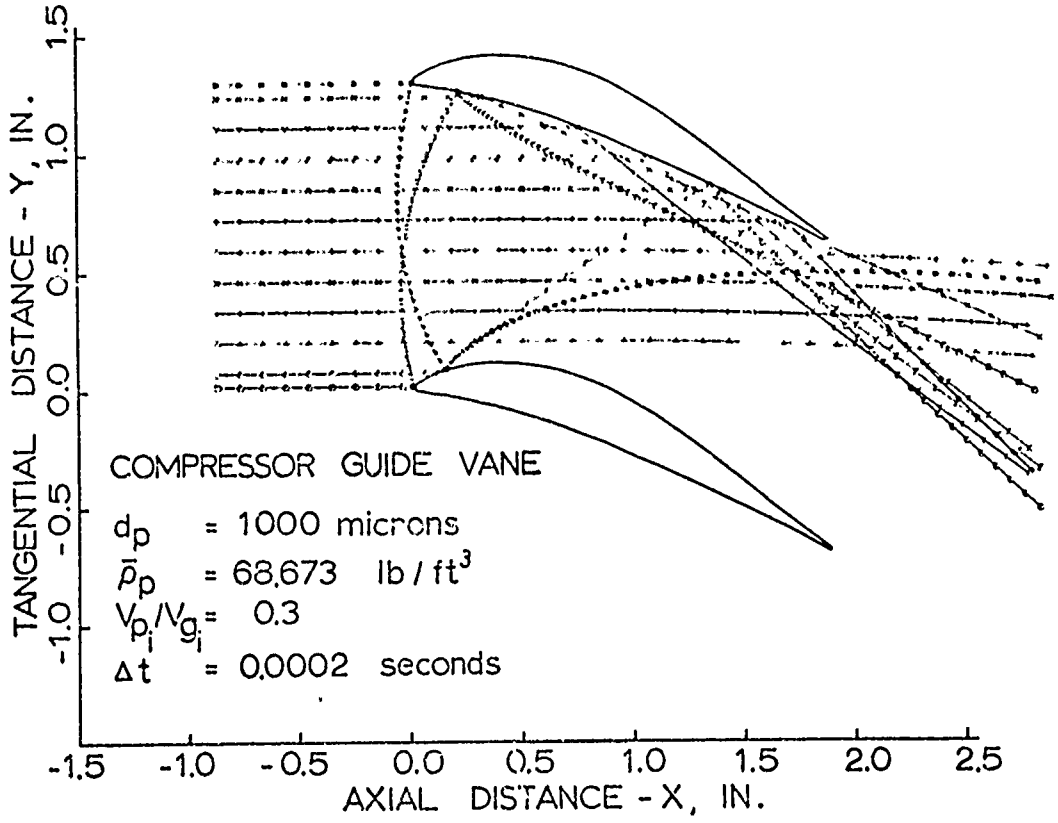

FIG.34 PARTICLE TRAJECTORIES

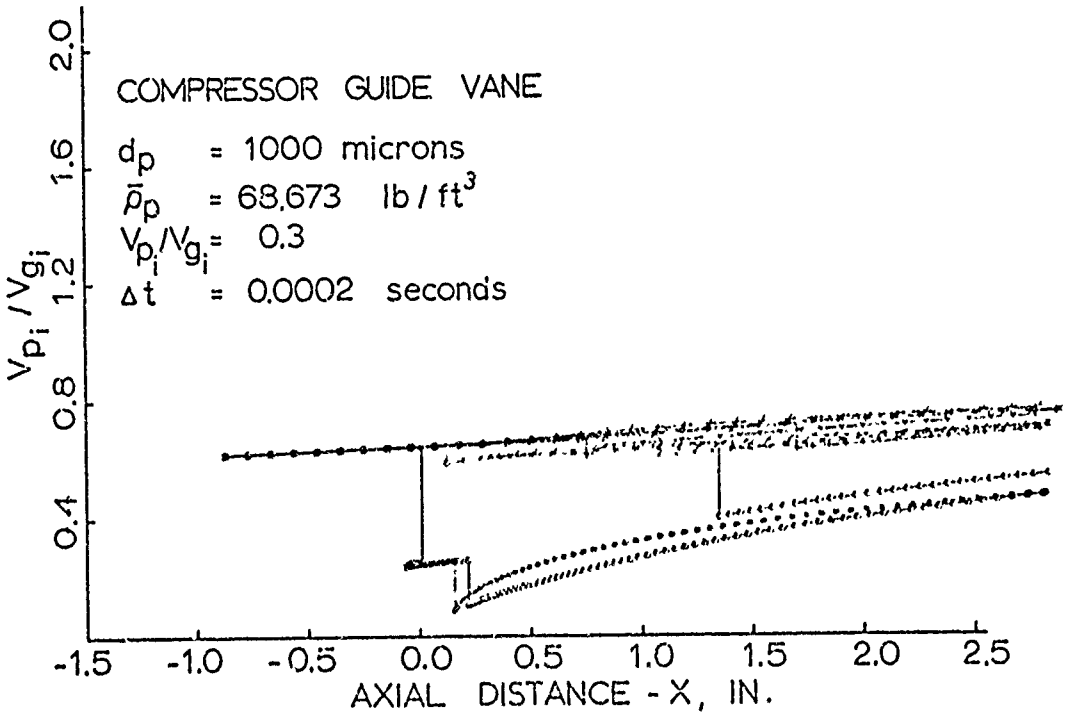

FIG. 35 PARTICLE NONDIMENSIONAL ABSOLUTE VELOCITY

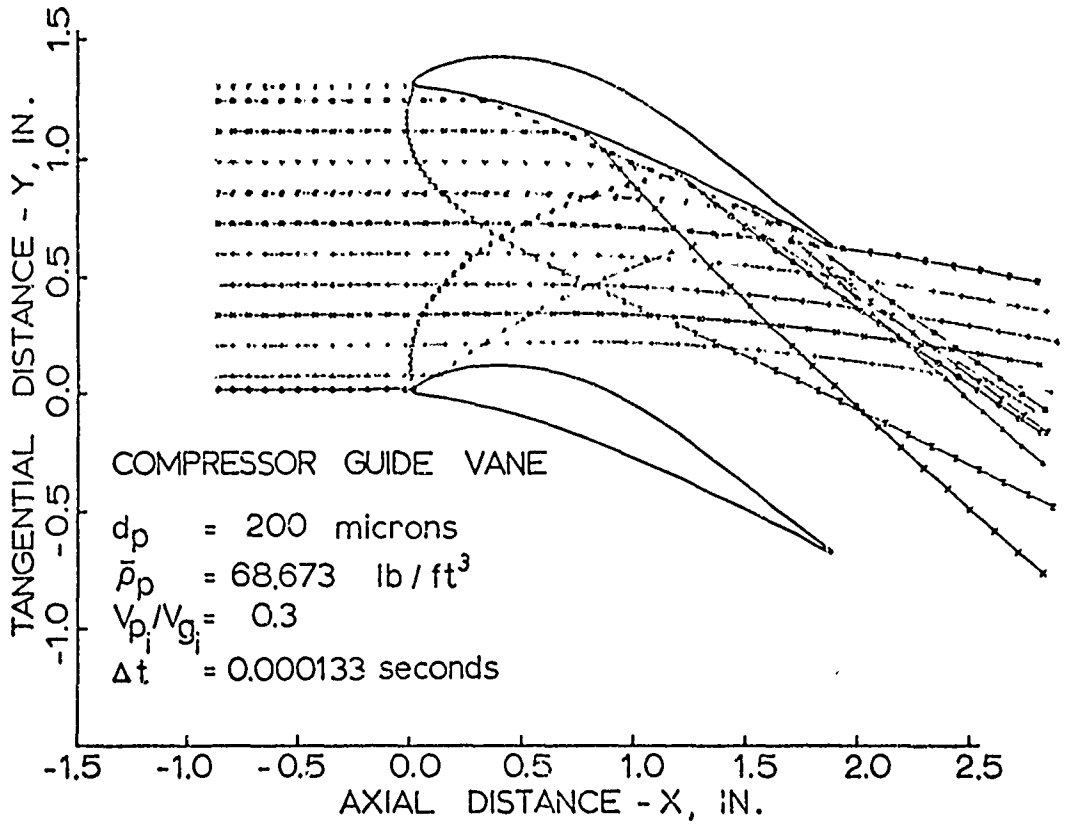

FIG. 36 PARTICLE TRAJECTORIES

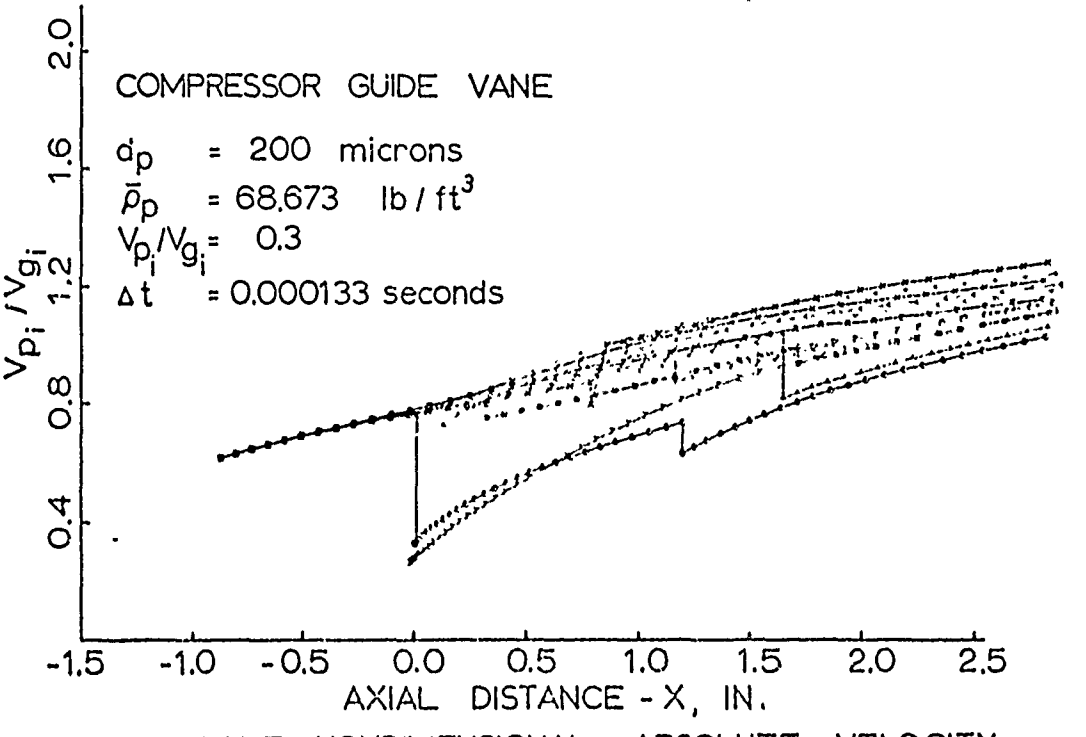

FIG.37 PARTICLE NONDIMENSIONAL ABSOLUTE VELOCITY

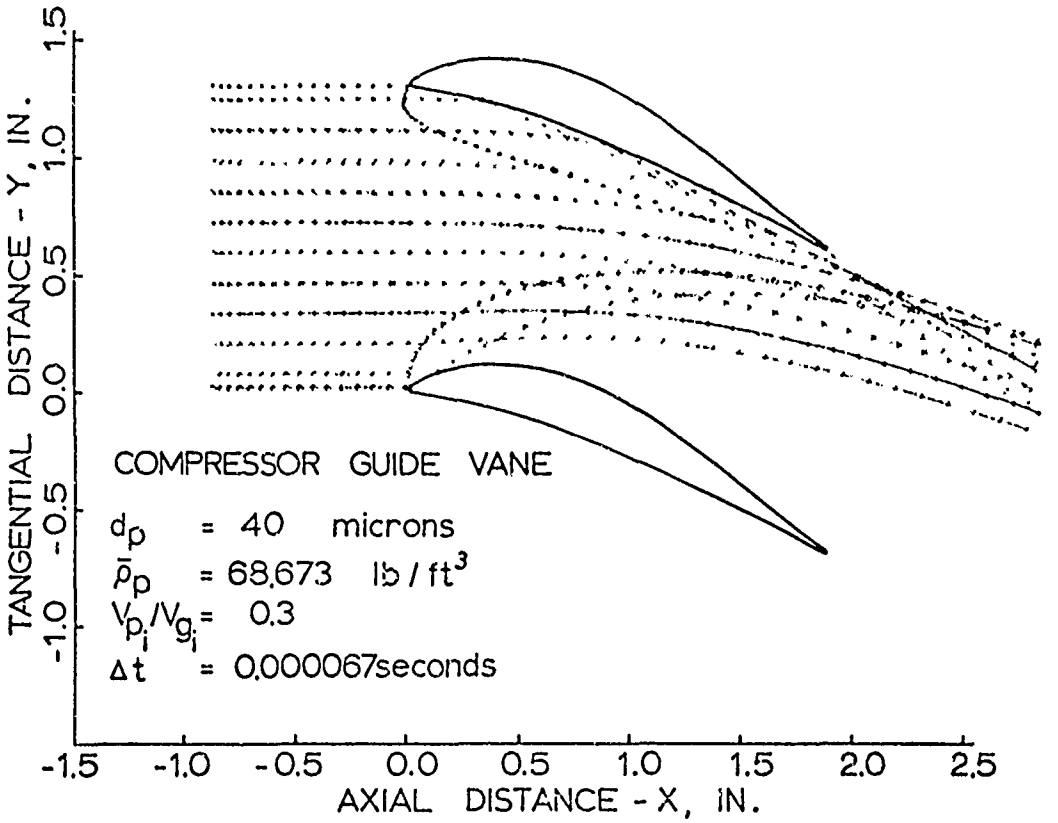

FIG.38 PARTICLE TRAJECTORIES

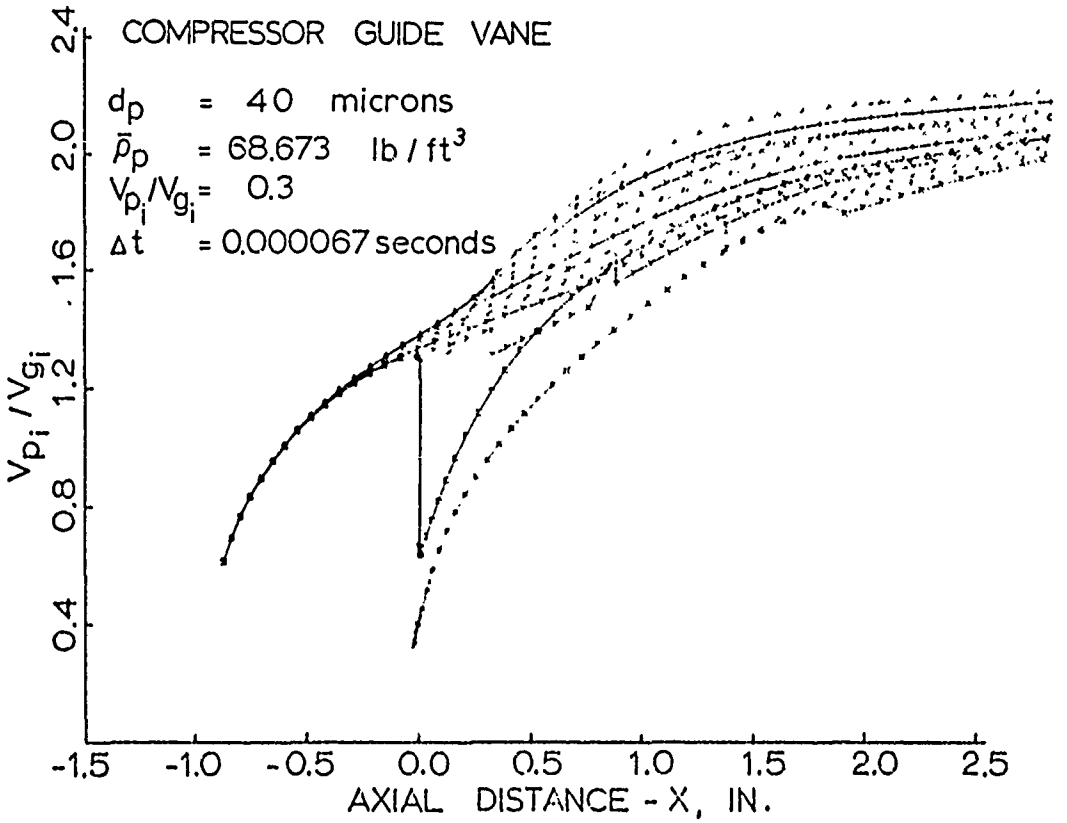

FIG.39 PARTICLE NONDIMENSIONAL ABSOLUTE VELOCITY